Stony Brook University

Simulation of Unexploded Ordnance Identification Using Tagged-neutron Interrogation and Neural Networks

A Thesis Presented

by

Xiaohai Zhu

to

The Graduate School

in partial fulfillment of the Requirements

for the degree of

Master of Science

In

Mechanical Engineering

Stony Brook University

May 2011

Stony Brook University

The Graduate School

Xiaohai Zhu

We, the thesis committee for the above candidate for the

Master of Science degree, hereby recommend

acceptance of this thesis.

Dr. Yu Zhou, Thesis Advisor
Assistant Professor, Mechanical Engineering Department

Dr. Chad Korach, Chairperson of Defense
Assistant Professor, Mechanical Engineering Department

Dr. Sudeep Mitra, Co-advisor
Nuclear Engineer, Department of Environmental Sciences, Brookhaven National Laboratory

This thesis is accepted by the Graduate School

Lawrence Martin

Dean of the Graduate School

Abstract of the Thesis

Simulation of Unexploded Ordnance Identification Using Tagged-neutron Interrogation and Neural Networks

by

Xiaohai Zhu

Master of Science

in

Mechanical Engineering

Stony Brook University

2011

This research is a collaboration between the Department of Mechanical Engineering at Stony Brook University and the Department of Environmental Sciences at Brookhaven National Laboratory. It is proposed to use 14 MeV neutrons tagged by the associated particle neutron time-of-flight technique (APnTOF) to identify the fillers of unexploded ordnances (UXO). The ultimate goal is to construct a prototype portable neutron interrogation probe that will search for UXO in a target volume, locate targets in three dimensions, and accurately identify the major elemental constituents. To facilitate the design of a prototype system, a preliminary simulation model was developed, using the Geant4 toolkit.

This work established the toolkit environment for generating tagged neutrons, their transport and interactions within a sample to induce emission, and detection of characteristic gamma-rays. Continuous coincident neutron and alpha fluxes were based on the Deuterium-Tritium fusion reaction principle which produces back-to-back emissions of neutrons and alpha particles of 14.1 and 3.5 MeV respectively. An algorithm has been developed for correlating the positions of alpha particles hitting the alpha detector with the tagged neutron and gamma-ray time-of-flight information, thereby making the system capable of 2D and 3D-image reconstruction of the interrogated object. The thesis demonstrates the novelty of the tagged-neutron approach for extracting useful signals of an object-of-interest with high signal-to-background ratio. Simulations indicated that an UXO filled with the RDX explosive, hexogen ($C_3H_6O_6N_6$), can be identified to a depth of 20 cm when buried in soil. The energy deposited in the detectors by gamma-rays from several elements and materials was recorded, and spectra were plotted. Neural networks were constructed with Matlab for spectra pattern identification. The results showed that the networks can effectively differentiate hexogen from other innocuous materials like nylon and PAN.

Table of Contents

List of Figures

List of Tables

Acknowledgements

I take this opportunity to thank my advisor, Prof. Yu Zhou, for his guidance and invaluable support throughout my academic pursuit at Stony Brook University. It is because of him that I have been able to successfully complete my thesis. I owe a lot to him. I would also like to extend my thanks to Dr. Sudeep Mitra for being as my co-advisor during this project. It is his tremendous research experience and valuable suggestions that have helped with completion of my work. Also I want to thank Prof. Chad Korach for being my thesis committee chair.

My parents have been my backbone and standing by me throughout. Without their encouragement and faith in my capabilities, all of this would not have been possible. Last but not the least, my dear friends at Stony Brook University made the experience a memorable one, and I cannot thank them enough.

As a graduate student of Stony Brook University in the past two years, I have learned so much and grown to a mature person. The environment here has been educating, inspiring and pleasant. I am now confident and well rounded in all specialties and I am looking forward to my endeavor for a brighter future.

Chapter 1

1 Introduction

1.1 Motivation

Cleaning up military sites suspected of containing munitions that have been armed and fired yet remain unexploded is one of the most pressing environmental problems. In particular, military downsizing after the Cold War has resulted in the closure of numerous military bases. Land that was once host to training ranges for such activities as firing practice and weapons testing is prepared for transfer to civilian ownership. The presence of unexploded ordnance (UXO) has interfered with the efforts to transfer and sell this land because of the potential hazards it poses to civilians [1].

The term “unexploded ordnance (UXO)” refers to any kinds of munitions that were fired but failed to explode upon impact; it can also refer to buried but long forgotten weapons caches or disposal sites [1]. Types of UXO span the full array of ammunition employed on the battlefield, including tank shells, artillery rounds, bombs, rockets, missiles, mortars, hand grenades, rifle grenades, bulk explosives, detonators, aircraft cannon, torpedoes, mines, pyrotechnics, chemical munitions, submunitions, and smallarms ammunition. UXO has posed a worldwide risk both in former combat areas and on military firing ranges. In US, the military tests and trains with live munitions to maintain readiness at all times; however, not all munitions detonate as designed. A large portion of UXO results from the failure of weapons fired during testing or training to

detonate, due to either a malfunction in the arming process or operator error. On average, the failure rate in the field is about 10 percent. Moreover, “for troop practice firings at training sites, there is normally no record of number of rounds fired vs. number of duds”, where a dud is an ammunition round or explosive that fails to fire or detonate on time or on command. This lack of record-keeping also increases the level of risk [2].

UXO presents both explosion and contamination risks. As long as UXO is in the ground, the risk of someone disturbing the munitions and causing an unexpected explosion remains. Hundreds of UXO-caused civilian injuries and deaths have been documented. It is expected that casualties will increase as civilians gain access to closed bases. Besides the obvious danger of explosion, buried UXO also entails the risk of environmental contamination. Munitions constituents include residue resulting from a munitions that has partially detonated, the open burning of excess explosives, the corrosion of UXO items, and the breakage of munitions without detonation. Common explosives that may remain in soil at former military training sites include trinitrotoluene (TNT), royal demolition explosive (RDX), high-melting explosive (HMX), and various isomers of dinitrotoluene (DNT) [2]. While the concentrations found in the study were generally low and decreased as the distance from the target areas increases, most ranges did have localized sources with high concentrations. Munitions chemicals can enter and contaminate groundwater. According to US Environmental Protection Agency (EPA) documents released in late 2002, UXO at 16,000 domestic inactive military ranges within the United States pose an “imminent and substantial” public health risk and could require the largest environmental cleanup ever, at a cost of at least $14 billion.

Range clearance operations must distinguish UXO filled with High Explosives (HE) from those with inert fillers, and non-destructive technologies are necessary for the cost-effective disposal of UXO during remediation of such sites. The only technique showing promise so far for the non-destructive elemental characterization of UXO fillers utilizes neutron interactions with the material. This method rests on the principle that explosives can be distinguished from each other and from innocuous materials by analyzing the quantities and ratios of carbon (C), nitrogen (N) and oxygen (O) in the material, particularly N which is unique to High Explosives (HE) [3].

Currently, the Pulsed Elemental Analysis with Neutrons (PELAN) exploits either or both of two types of neutron interactions with nuclei, (a) inelastic scattering and (b) neutron capturing, and then detects the induced element-specific high-energy prompt gamma-rays [4]. However, several unresolved issues hinder the wide application of this potentially very suitable technique. The most important one is that neutrons interact with all surrounding matter in addition to the interrogated material, leading to a very high gamma-ray background in the detector. Systems requiring bulky shielding and having poor signal-to-noise ratios (SNRs) for measuring elements are unsuitable for field deployment.

1.2 Proposed Methods

The inadequacies of conventional neutron interrogation methods are overcome by using the tagged-neutron approach, and the availability of compact sealed neutron generators exploiting

this technique [5,6] offers field deployment of non-intrusive measurement systems for detecting threat materials, like explosives and drugs [7]. By accelerating deuterium ions into a tritium target, the subsequent fusion reaction generates nearly back-to-back emissions of neutrons and alpha particles of energy 14.1 and 3.5MeV respectively. A position-sensitive detector recognizes the associated alpha particle, thus providing the direction of the neutron; The time-of-flight is determined by the alpha-gamma coincidence time. The neutrons associated with the detection of an alpha particle are called tagged neutrons. Tagged neutrons interact with the nuclei of the interrogated object, producing element-specific prompt gamma-rays that the gamma detectors recognize. Measuring the delay between the detections of the alpha particle and the time-of-arrival of gamma-ray determines where the reaction occurred along the axis of the neutron beam (14.1 MeV neutrons travel at 5 cm/nanosecond, while gamma rays cover 30 cm/nanosecond). The main advantage of the technique is its ability to simultaneously provide 2D and 3D imaging of objects and their elemental composition. Since the technique involves electronic collimation of the neutron beam, compact field deployable systems can be built (Fig. 1.1).

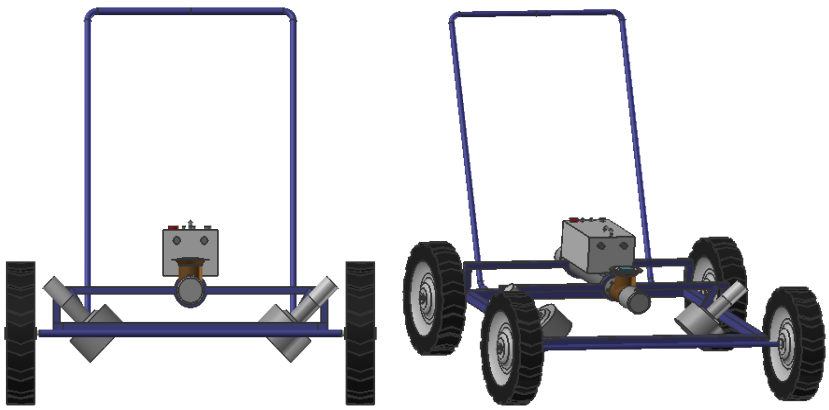

Figure 1.1: Concept model of the explosive detection equipment

To facilitate the design and construction of a prototype tagged-neutron system, simulations were developed using the Geant4 toolkit [8], which is an open source program developed for particle physics. There are a growing number of high energy physics experiments that use the technology provided by this program in the preparation of the detector and the interpretation of the data. The toolkit utilizes object-oriented technology and was developed at CERN, Geneva for simulating high-energy particle interactions with matter and detector responses in such experiments. It was selected in the present study for tagged-neutron simulations because of its versatile geometry, material definition packages and graphic routines which enable on-line monitoring of the geometric details of the volumes and of the particle tracks.

The thesis is organized as follows to discuss in detail:

- The installation of GEANT4 simulation platform for different hardware systems is presented in Chapter 2
- A description of D+T reaction principle as well as generation of tagged neutrons by Geant4 can be found in the beginning of Chapter 3. Then, this chapter addresses several models to simulate the nature of the alpha-gamma coincidence time spectra and their use for isolating gamma-ray spectra of an object-of-interest from its surrounding in simple and complex situations. There is also a model to simulate the image reconstruction of the interrogated object using the neutron and gamma-ray time-of-flight information.
- To simulate the experimental results more closely, electromagnetic processes that govern a variety of photon interactions within the active detector volume are

implemented in the simulation environment. Such generated spectra of energy deposited by gamma-rays from different elements and materials are used as the data base for pattern identification. These will be discussed in Chapter 4.

- Chapter 5 focuses on the establishment of neural network with Matlab, training process and result analysis of recognizing several sample materials.
- The final chapter summarizes the work of this research and makes a few points regarding the future development of this work.

Chapter 2

2 Simulation Platform Developed with Geant4

2.1 Introduction to GEANT4

GEANT4 is a free software package composed of tools which can be used to accurately simulate the passage of particles through matter [9]. It was developed at CERN for high-energy, nuclear and accelerator physics, as well as studies in medical and space sciences. GEANT4 uses the C++ object-oriented computer language. Users can implement the description of the geometry and the materials of the detector, particle transport and the physics processes of interaction with materials and a particle generator with flexible visualization of geometries, tracks and interactions.

All aspects of the simulation process have been included in the toolkit:

- the geometry of the system,
- the materials involved,
- the fundamental particles of interest,
- the generation of primary events,
- the tracking of particles through materials and electromagnetic fields,
- the physics processes governing particle interactions,
- the response of sensitive detector components,
- the generation of event data,

- the storage of events and tracks,
- the visualization of the detector and particle trajectories, and
- the capture and analysis of simulation data at different levels of detail and refinement.

Users may construct stand-alone applications or applications built upon another object-oriented framework. In either case the toolkit will support them from the initial problem definition to the production of results and graphics for publication.

At the heart of GEANT4 is an abundant set of physics models to handle the interactions of particles with matter across a very wide energy range. Data and expertise have been drawn from many sources around the world and in this respect, GEANT4 acts as a repository which incorporates a large part of all that is known about particle interactions.

In object-oriented analysis class categories are used to create logical units. The class category diagram designed for GEANT4 is shown in the figure below. Each box in Fig. 2.1 represents a class category, and a "uses" relation by a straight line. The circle at an end of a straight line means the class category which has this circle uses the other category [8].

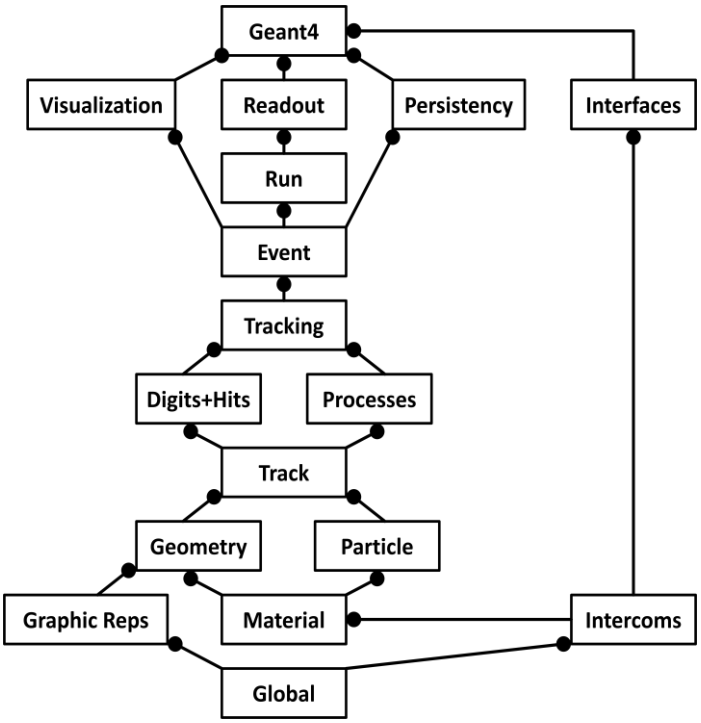

Figure 2.1: GEANT4 class categories

The following is a brief summary of the role of each class category in GEANT4 [8].

1) Run and Event

These are categories related to the generation of events, interfaces to event generators, and any secondary particles produced. Their roles are principally to provide particles to be tracked to the Tracking Management.

2) Tracking and Track

These are categories related to propagating a particle by analyzing the factors limiting the step and applying the relevant physics processes. The important aspect of the design was that a generalized GEANT4 physics process (or interaction) could perform actions, along a tracking step, either localized in space, or in time, or distributed in space and time (and all the possible combinations that could be built from these cases).

3) Geometry and Magnetic Field

These categories manage the geometrical definition of a detector (solid modeling) and the computation of distances to solids (also in a magnetic field). The GEANT4 geometry solid modeler is based on the ISO STEP standard and it is fully compliant with it, in order to allow in future the exchange of geometrical information with CAD systems. A key feature of the GEANT4 geometry is that the volume definitions are independent of the solid representation. By this abstract interface for the G4 solids, the tracking component works identically for various representations. The treatment of the propagation in the presence of fields has been provided within specified accuracy. An OO design allows us to exchange different numerical algorithms and/or different fields (not only B-field), without affecting any other component of the toolkit.

4) Particle Definition and Matter

These two categories manage the definition of materials and particles.

5) Physics

This category manages all physics processes participating in the interactions of particles in matter. The abstract interface of physics processes allows multiple implementations of physics models per interaction or per channel. Models can be selected by energy range, particle type, material, etc. Data encapsulation and polymorphism make it possible to give transparent access to the cross sections (independently of the choice of reading from an ascii file, or of interpolating from a tabulated set, or of computing

analytically from a formula). Electromagnetic and hadronic physics were handled in a uniform way in such a design, opening up the physics to the users.

6) Hits and Digitization

These two categories manage the creation of hits and their use for the digitization phase. The basic design and implementation of the Hits and Digitization had been realized, and also several prototypes, test cases and scenarios had been developed before the alpha-release. Volumes (not necessarily the ones used by the tracking) are aggregated in sensitive detectors, while hits collections represent the logical read out of the detector. Different ways of creating and managing hits collections had been delivered and tested, notably for both single hits and calorimetry hits types. In all cases, hits collections had been successfully stored into and retrieved from an Object Data Base Management System.

7) Visualization

This manages the visualization of solids, trajectories and hits, and interacts with underlying graphical libraries (the Visualization class category). The basic and most frequently used graphics functionality had been implemented already by the alpha release. The OO design of the visualization component allowed us to develop several drivers independently, such as for OpenGL and OpenInventor (for X11 and Windows), DAWN, Postscript (via DAWN) and VRML.

8) Interfaces

This category handles the production of the graphical user interface (GUI) and the interactions with external software (OODBMS, reconstruction etc.).

2.2 Geant4 Platform on Windows

Three pieces of software are required for building Geant4 on Windows [10].

- Microsoft C++ is the compiler that is recommended for Geant4 on Windows.
- Cygwin is a Linux shell environment that runs on top of Windows. By requiring Cygwin, we obtain a common, Linux-like baseline for all of our users. This greatly simplifies installation and configuration support. While the Cygwin compiler does work for Geant4, the Microsoft compiler produces significantly faster-running code. The Microsoft compiler is therefore the officially supported Geant4 solution.
- CLHEP is a set of base libraries that have long provided great functionality for the particle physics community. They provide things like matrix manipulations, four-vector tools and lists of particle properties.

In our research, the Geant4 version 4.9.3.p01 was implemented for Windows. A Lenovo T400 computer with an Intel processor running at 2.26 GHz and a 1.58 GHz, 2 GB RAM was used as the hardware on which Windows XP Professional 2002, service pack 3 was installed.

2.3 Geant4 Platform on Linux

Two pieces of software required for building Geant4 on Linux [10].

- gcc is the compiler that is recommended for Geant4 on Linux.
- CLHEP

In our research, the Geant4 version 4.9.4 was implemented for Linux. A Dell computer with two Intel(R) Core(TM)2 Duo CPU E4600 processors running at 2.46 GHz and a 3.6 GB RAM was used as the hardware on which Ubuntu Desktop Edition 10.10, 32 bit, gcc4.4.5 was installed.

Ubuntu is not listed as one of the recommended Linux versions on the official website of Geant4. So, you may have some problems installing Geant4 on Ubuntu. The following is a brief summary of the installation process.

1) make sure you have installed all of the system updates
2) Install the basic compiling environment: sudo apt-get install build-essential
3) Install OpenGL Library: sudo apt-get install libgl1-mesa-dev
4) Install OpenGL Utilities: sudo apt-get install libglu1-mesa-dev. OpenGL Utilities is a tool set based on OpenGL Library, and provides many convenient functions, making OpenGL easier to use.
5) Install libxt-dev: sudo apt-get install libxt-dev. If the package was not installed, compiling would get error: “X11/Intrinsic.h: No such file or directory”
6) Install libxi-dev: sudo apt-get install libxi-dev. Otherwise, compiling would get error: “/usr/bin/ld: cannot find –lXi”
7) Install zlib1g-dev: sudo apt-get install zlib1g-dev. Otherwise, compiling would get error: “zlib.h: No such file or directory”

8) Look for “libxmu” in “Synaptic Package Manager”, and Install the 7 found results. Otherwise, compiling would get error: “include/G4OpenGLXViewer.hh: 46: 29: error: X11/Xmu/StdCmap.h: No such file or directory”.

9) Open “Synaptic Package Manager” of Ubuntu, look for “geant”, and install the 6 results. They are the packages used for physics.

10) Then you can continue with the following installation based on the instruction on the official website of Geant4.

Geant4 can also be installed on Mac. But it is not implemented in our research.

Chapter 3

3 Tagged-neutron Approach and Applications

3.1 Generation of Tagged Neutrons

Simulations of this chapter were all conducted on the Geant4 platform installed on Windows.

The most common type of fusion reaction discussed for fusion energy in the near future is the fusion of two hydrogen isotopes: deuterium (^{2}H) and tritium (^{3}H). It is the easiest fusion reaction to achieve on Earth, and will most likely be the type of reaction found in first generation fusion reactors [11]. Figure 3.1, shows the actual reaction involves a deutrerium nucleus fusing with a tritium nucleus to form an alpha particle(^{4}He nucleus) and a neutron. The products contain around 17.6 million electron volts (MeV) of released kinetic energy through the loss of mass in the fusion process(see Eqn.3.1)[11].

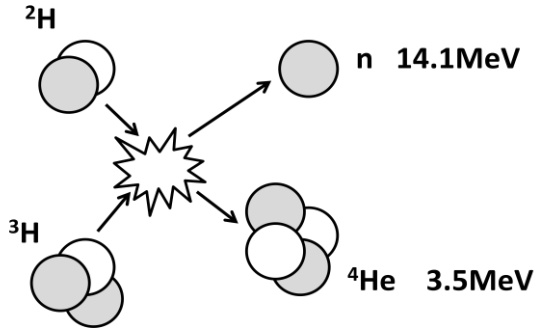

Figure 3.1: D+T reaction

$$^2_2H + ^3_3H \rightarrow ^4_2He + ^1_0n + 17.6MeV \qquad \text{Eqn.3.1}$$

The D-T reaction is the easiest because the extra neutrons on the nuclei of the deuterium and tritium increase their size and thus the probability of a fusion reaction. They also each have the smallest possible positive charge (since hydrogen has only one proton), making it relatively easy to have the two nuclei overcome their repulsion and fuse together.

Consider the following two-body reaction, see Fig.3.2. Initially nucleon 1 is incident on nucleon 2 which is at rest in the lab system; after the interaction nucleons 3 and 4 emerge.

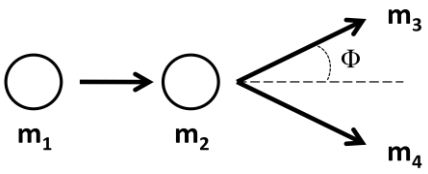

Figure 3.2: Two-body reaction.

The general expression for the energy of nucleon 3 in the lab system can be written in the form [12]:

$$E(m_3,\phi)=\left(\frac{m_1}{m_1+m_2}\right)^2\frac{m_3}{m_1}E_0\cos 2\phi\,\frac{m_4}{m_3+m_4}\left(\frac{m_2}{m_1+m_2}E_0+Q\right)$$
$$\pm\frac{2\cos\phi}{m_1+m_2}\sqrt{m_1m_3\frac{m_4}{m_3+m_4}E_0\left(\frac{m_2}{m_1+m_2}E_0+Q\right)} \qquad \text{Eqn.3.2}$$
$$\times\sqrt{1-\frac{m_1m_3}{m_1+m_2}\frac{E_0\sin^2\phi}{m_4\left(\frac{m_1m_3}{m_1+m_2}E_0+Q\right)}}$$

Where E_0 is the energy of nucleon 1 in the lab system, Φ is the lab angle made by the velocity vector of nucleon 3 with the beam direction, the m_i's are the respective nucleon masses, and the Q of the reaction is defined customarily as $Q = m_3+m_4-m_1-m_2$.

For the case of the reaction d + T → n + ^{4}He, Eqn. 3.2 yields for the neutron energy [12]:

$$E(E_0,\phi_n) = 0.08E_0\cos 2\phi_n + 0.8\left(0.6E_0 + 17.6\right)$$
$$+ 0.8\cos\phi_n\sqrt{0.4E_0\left(0.6E_0 + 17.6\right)} \times \sqrt{1 - \frac{E_0 \sin^2\phi_n}{10\left(0.6E_0 + 17.6\right)}} \qquad \text{Eqn.3.3}$$

Where Q= 17.6 MeV, standing for the total released kinetic energy.

In the lab frame of reference, the neutron and associated α-particle from a given D-T encounter are to be found. Eq. 3.4 [12] relates Φ_α, the angle made by the α-particle with beam direction, to Φ_n, that made by the neutron and the beam direction (Fig.3.3).

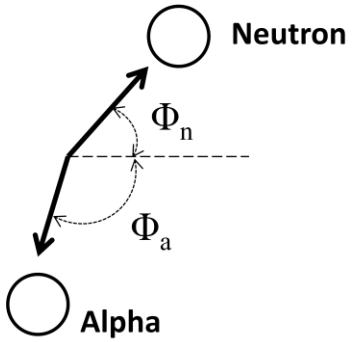

Figure 3.3: Angle between alpha particle and incident beam for deuteron bombarding energy E_0

$$\tan\phi_\alpha = \frac{\frac{1}{2}\sin 2\phi_n + \sin\phi_n\sqrt{\frac{1}{\gamma^2} - \sin^2\phi_n}}{-\sin^2\phi_n + \cos\phi_n\sqrt{\frac{1}{\gamma^2} - \sin^2\phi_n} - \frac{m_\alpha}{m_n}} \qquad \text{Eqn.3.4}$$

Where $\frac{1}{\gamma^2} = \frac{V_n}{V_{c.m.}} = \frac{m_\alpha}{m_n}\frac{(m_1+m_2)}{m_1}\left(\frac{m_2}{m_1+m_2} + \frac{Q}{E_0}\right)$

m_1= mass of incident particle

m_2= mass of target particle

m_n= mass of neutron

m_α = mass of alpha

E_0 = incident energy

In Table 3.1, Eqn. 3.4 has been evaluated for several values of the deuteron bombarding energy, E_0.

Table 3.1: Angle between alpha particle and incident beam for deuteron bombarding energy E_0

Φ_n (lab) °	E_0=0.1MeV	E_0=0.2MeV	E_0=0.3MeV	E_0=0.4MeV	E_0=0.5MeV
0	180 °	180 °	180 °	180 °	180 °
10	168°41’	168° 04’	167° 36’	167° 06’	166° 40’
20	157°26’	156°14’	154° 58’	154 °22’	153° 33’
30	146° 17’	144° 34’	143° 10’	141° 56’	140° 48’
40	135° 17’	133° 08’	131° 24’	129°54’	128° 32’
50	124° 27’	121° 58’	120° 01’	118° 19’	116° 48’
60	113° 49’	111° 07’	109° 01’	107° 13’	105° 37’
70	103° 24’	100° 36’	98° 26’	96° 36’	94 °59’
80	93° 12’	90° 22’	88° 13’	86° 25’	84° 51’
90	83° 12’	80° 27’	78° 23’	76° 39’	75° 10’
100	73° 25’	70° 48’	68° 51’	67° 16’	65° 53’
110	63° 49’	61° 24’	59° 58’	58° 11’	56° 56’
120	54° 22’	52° 14’	50° 39’	49° 23’	48° 17’
130	45° 05’	43° 14’	41°53’	40° 48’	39° 53’
140	35° 55’	34° 24’	33° 18’	32° 25’	31° 40’
150	26°51’	25° 41’	24° 51’	24° 11’	23° 37’

160	17° 51’	17° 04’	16° 31’	16° 04’	15° 31’
170	8°55’	8° 31’	8° 12’	8° 00’	7° 49’
180	0	0	0	0	0

In T(d,n) ^{4}He reaction, generally, the tritium target is fixed with zero initial energy. It is interesting to note that the initial energy of deuterium E_0 will affect the folding angle between neutron and alpha particle (θ_{na}). If both D and T are at rest, the generated neutron and alpha will be moving exactly in opposite direction. Since the deuterium energy of most portable commercial neutron generators works around 0.1 MeV, we will only simulate situation when E_0 = 0.1 MeV. The folding angle between neutron and alpha particle θ_{na} is ideally considered to be 180 °.

D+T reaction provides us neutron at 14.1 MeV and alpha particle at 3.5 MeV with opposite direction when the initial energy of D, E_0 is 0.1 MeV. Using particle guns designed in the Geant4 primary generator, a neutron of energy 14.1 MeV and its associated alpha particle with energy 3.5 MeV were generated at the same time and in opposite directions. The azimuthal angle φ of both particles is uniformly distributed and generated randomly within 360^o. The cone angle θ is constrained to be no larger than ±45 °.

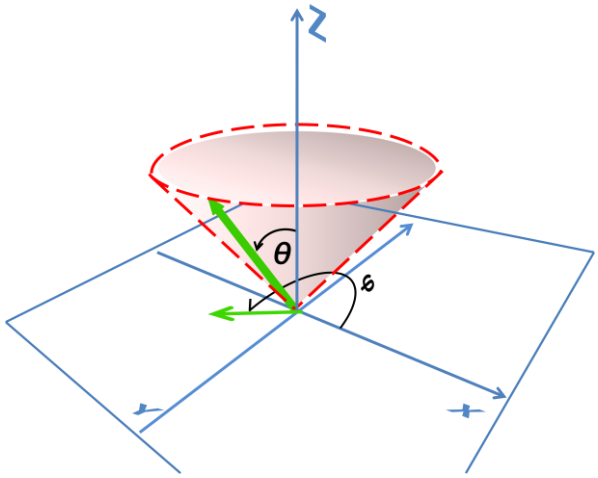

Figure 3.4: The azimuthal angle φ of both neutrons and alphas is uniformly distributed within 360^{o}; The cone angle θ is constrained to be within ±45 °.

3.2 Physical lists Associated with Neutron Interrogation

A user class was derived from G4PhysicsList, in which we could implement the physical processes to be used in our simulations. Neutrons were transported using the LHEP_PRECO_HP, Hadronic physics list. This is suitable for elastic and inelastic scattering of neutrons with energy < 20 MeV. We use the G4NDL evaluated neutron data library for cross sections.

3.3 Model Experiments of Neutron Interrogation

3D world volume was defined and filled with vacuum. All components of the system were placed within it. The neutron and alpha particle production site was placed at the origin of the world volume at the center of the box using an x, y and z Cartesian coordinate system where the z axis was the alpha particle and neutron directions (Fig.3.5).

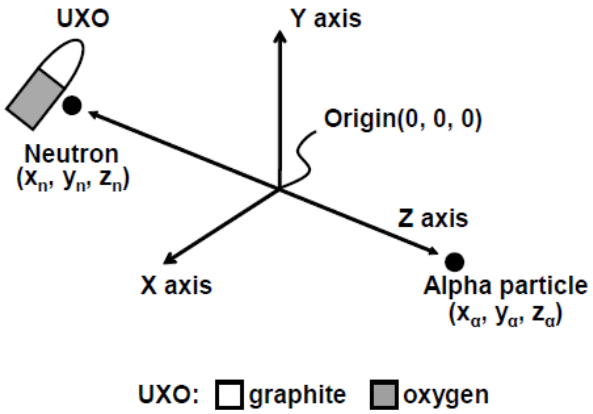

Figure 3.5: Geometry of the associated-particle neutron time-of-flight technique showing the cartesian coordinate system where position sensing of the alpha particle in the (x,y) plane allows the determination of the neutron trajectory in the same plane along the z axis.

Using particle guns designed in the Geant4 primary generator, a neutron of energy 14.1 MeV and its associated alpha particle with energy 3.5 MeV were generated at the same time and in opposite directions. The azimuthal angle φ of both particles was uniformly distributed and generated randomly within 360^0. The cone angle θ_n was constrained to be no larger than $\pm 45^0$. For all experiments, 100,000 alpha-neutron pairs were used in each run. The computation time was ~20 minutes for each run.

Several models have been developed in this environment to simulate the nature of the alpha-gamma coincidence time spectra and their use for isolating gamma-ray spectra of an object-of-interest from its surrounding in simple and complex situations.

- Model 1: a simulation to mimic two objects that are within the cone of tagged neutrons but separated by a finite gap between them.

An alpha-particle detector made up of plastic and having a diameter of 30 cm and thickness 1 cm was placed at the position (0,0,30) cm and two NaI gamma-ray detectors each of diameter

60 cm and thickness 15 cm were positioned at (50,0,30) cm and (-50,0,30) cm relative to the origin of the world volume. The large sizes of the detectors were designed for better solid angle coverage. The detectors were also defined to be sensitive so that once a particle entered the detector, it recorded all the necessary hit information such as position and time. The events in the two gamma-ray detectors were summed for enhancing the counting statistics. Soil composition was represented by SiO_2, and graphite by C with densities 1.2 and 1.7 g cm^{-3}, respectively. The object-of-interest, graphite sample was 30 cm x 30 cm x 20 cm thick and placed 75 cm from the neutron production site. The soil piece is of the same size. The lower surface of the soil and the upper surface of the objects-of-interest were separated by a distance of 30 cm (Fig. 3.6).

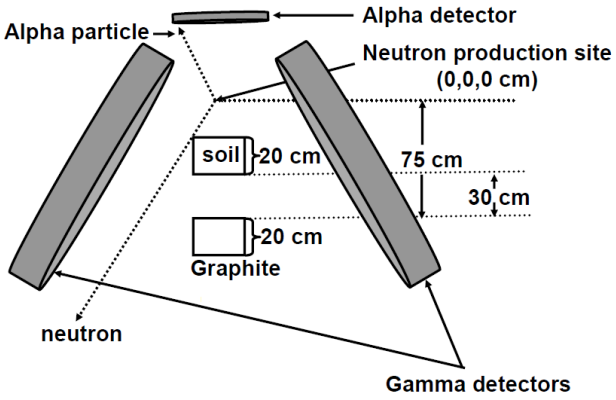

Figure 3.6: Top view of the simulation environment of model 1, showing the placement of objects along the neutron beam axis.

In model 1, the centers of the two objects, soil and graphite, were separated by 50 cm and the simulation correctly tracked the 14.1 MeV neutrons to the two objects; the centroids of the two neutron time-of-flight (TOF) peaks were separated by ~10 ns as predicted from theory, because the speed of a 14.1 MeV neutron is 5.1 cm/ns. So, appropriate time windows 1 and 2 of the two TOF peaks (Fig.3.7a) revealed that the associated gamma-rays were from soil and

graphite respectively. The characteristic C signal at 4.43MeV from graphite was not seen in the gamma-rays from window 1. Similarly, window 2 showed only the C signal and the soil signals were eliminated based on the neutron time of-flight. The simulation also correctly produced the major prompt inelastic gamma-ray peaks from Si and O of soil and the single excited peak of C.

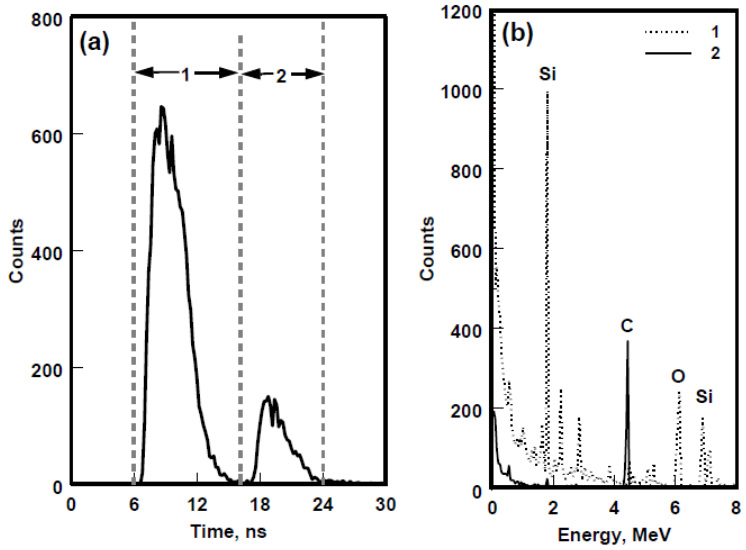

Figure 3.7: (a) Time distribution of gamma-rays from the two objects, soil and graphite when separated by a gap of 30 cm and (b) the associated time correlated gamma-ray spectra using windows 1 and 2 showing that signals from the two objects in the neutron field can be completely separated.

- Model 2: two objects within the defined cone are contiguous to each other

For the contiguous case, the soil layer was displaced by 30 cm toward the graphite block to make contact with it (Fig. 3.8).

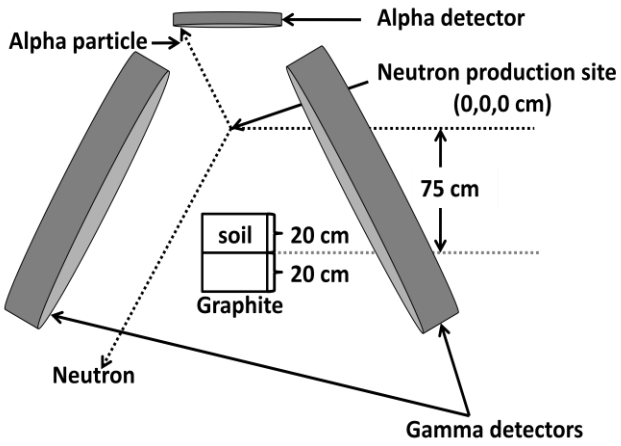

Figure 3.8: Top view of the simulation environment of model 2, showing the placement of objects along the neutron beam axis.

For model 2 where the two objects were in contact, the nature of the time peak changed to a single peak as expected and would be similar to the case if a single object was present at that position, i.e., the gamma-ray energies contributing to the TOF spectrum is a combination of all nuclei located in that region. However, when appropriate time slices were selected as shown in Fig.3.9a corresponding to different neutron flight times, the associated gamma-ray energies revealed that signals from window 1 were due to the soil covering the graphite whereas signals from time window 2 were from C. It must be mentioned that the C signal intensity in window 2 is of much lower intensity compared to the gap case in model1 because the time window selected was much narrower so as to eliminate the overlap region in the time peak from the two objects in the contiguous case of model 2.

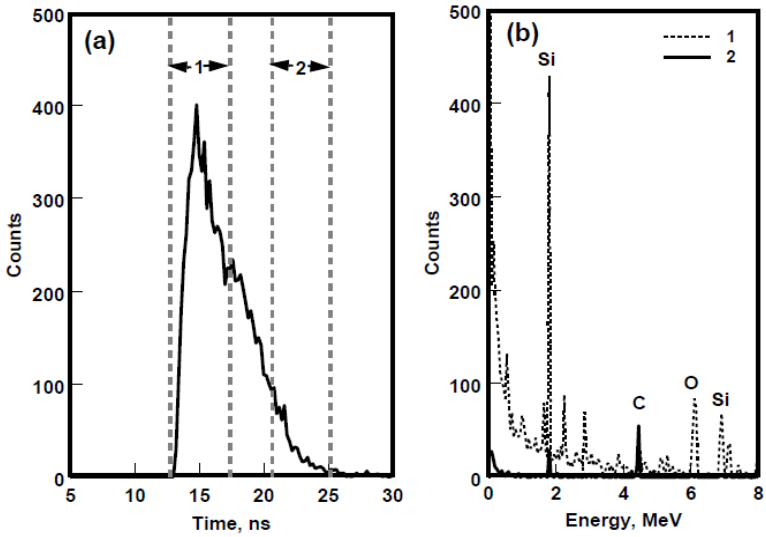

Figure 3.9: (a) Time distribution of gamma-rays for the case when the soil and graphite samples are contiguous and (b) the associated gamma-rays for time slices 1 and 2 clearly separating the signals due to the two objects

- Model 3: a common HE like hexogen ($C_3H_6O_6N_6$) is buried in soil to various depths

This model addressed the need for the identification of UXO in the sub-surface. Soil composition was represented by SiO_2, and hexogen as $C_3H_6O_6N_6$ with densities 1.2 and 1.8 g cm^{-3}, respectively. The hexogen sample was 30 cm x 30 cm x 20 cm thick and placed 75 cm from the neutron production site. As a simple case, the soil cover was separated from the hexogen sample so that the time peaks from the two objects could be easily resolved as in model 1. However, soils of different thicknesses were added layer-wise towards the neutron production site in model 3(Fig.3.10).

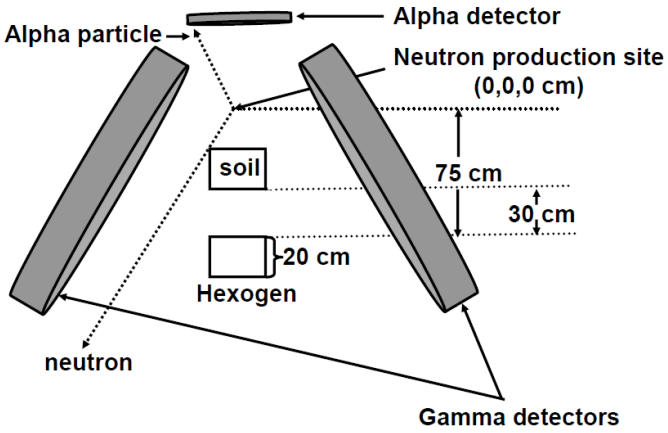

Figure 3.10: Top view of the simulation environment of model 3, showing the placement of objects along the neutron beam axis.

The time peak intensity of soil increased, because the neutron-induced inelastic gamma-rays from the amount of soil also increased with increasing thickness. The time peak at ~19 ns representing the hexogen sample reduced progressively with increasing soil thickness (Fig.3.11). This can be mainly attributed to the neutron's attenuation in soil.

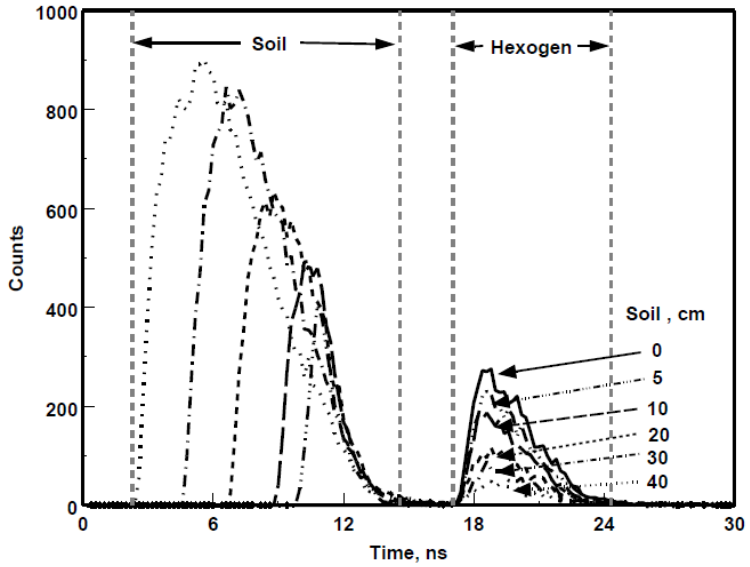

Figure 3.11: Time distribution of gamma-rays from soil and the hexogen sample showing the expected decrease in the hexogen time peak intensities with increasing soil thickness due to the neutron attenuation in the soil.

As control experiments, a neutron sensitive detector made up of plastic and dimensions 30 x 30 x 1 cm thick was defined to monitor the uncollided fraction of 14 MeV neutrons at the position of the object-of- interest. The top surface of the detector was likewise 75 cm from the neutron production site (Fig.3.12).

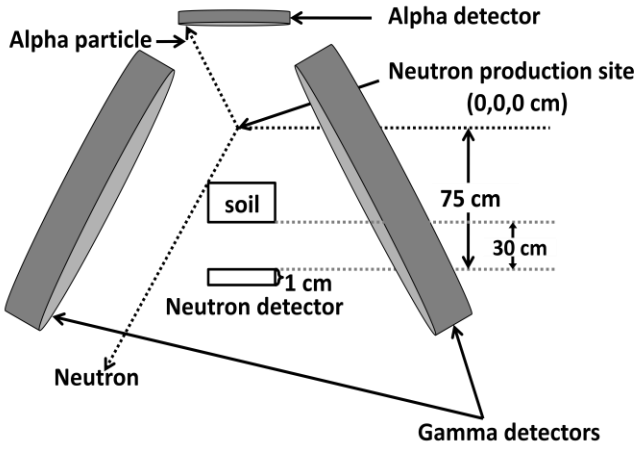

Figure 3.12: Top view of the simulation environment of neutron detector, showing the placement of objects along the neutron beam axis.

The variation of the neutron intensity with soil thickness as registered by the neutron sensitive detector at the hexogen position is shown in Fig. 3.13 along with the drop in gamma-ray intensities of C, N and O at 4.43, 5.1 and 6.13 MeV respectively. To check that these results produced by Geant4 were meaningful, the soil was replaced by various thicknesses of water and the uncollided fractions of 14 MeV neutrons were determined. The half-value thickness of 14.1 MeV neutrons in water was simulated to be 10.4 cm (Fig.3.13). This compared favorably with the experimentally determined value of 9.2 $\pm$ 1.1 cm [13]. The mean C/N counts ratio from the gamma-rays of hexogen associated with the neutron TOF (time window 2) was 2.76 ($\pm$ 0.11, CV, 3.9 %) to a depth of 20 cm in soil. However, between 20-40 cm depth, the

uncertainties in the mean value of the ratio became very significant; it was 2.45(±0.6, CV, 25%). The findings indicate that the identification of filler material will become particularly difficult for those UXO filled with HE and buried to greater than 20 cm depths in the sub-surface.

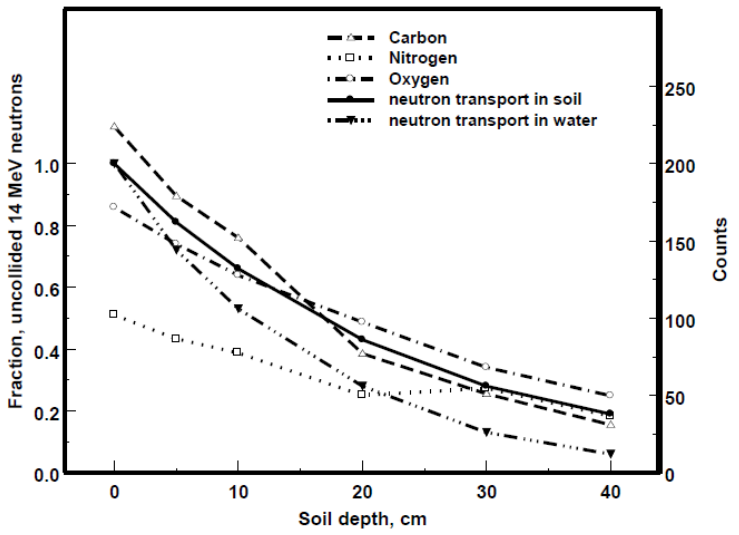

Figure 3.13: The fraction of uncollided 14 MeV neutrons decreased with increasing soil thickness (as a result, the gamma-ray intensities of hexogen also decreased). When the neutrons were tracked in water, a half-value thickness of 10.4 cm was obtained.

- Model 4: 2D and 3D imaging of interrogated object using the neutron and gamma-ray time-of-flight information

For simulating the imaging, the long axis of a cylindrical "bomb-shaped" object of diameter 20 cm and length 25 cm was placed perpendicularly to the neutron beam axis at a distance of 20 cm from the neutron production site. One half of the cylinder was filled with graphite and the other half was filled with solid oxygen having density as 1.43g cm^{-3} (Fig. 3.14).

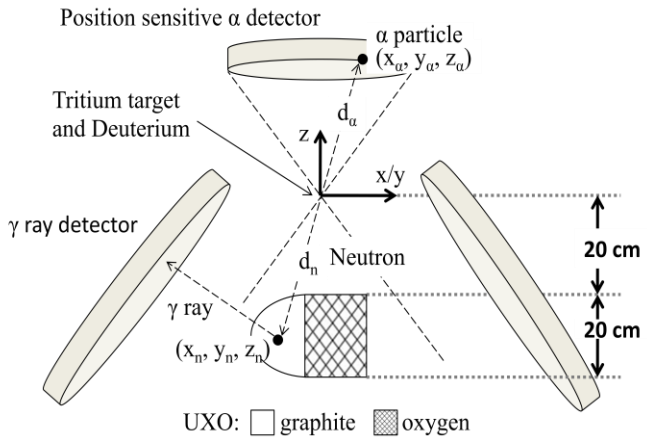

Figure 3.14: Top view of the imaging reconstruction model

Geant4 can record the x,y,z position of an alpha hitting on the alpha detector (x_a, y_a, z_a), energy deposited by a gamma E_g, and Time-of-Arrival of a gamma t_g. To be specific, t_g stands for the time from the start of neutron emission, interaction with the nuclei and generation of a gamma-ray, to its hitting on the gamma detector. d_n stands for the distance from the source origin to the reaction point along the axis of a neutron beam. d_a is the distance from the source origin to an alpha's hitting on the detector. Eqn.3.5 calculates the velocity of alpha and neutron particles as V_a=1 cm/nanosecond, and V_n=5 cm/nanonsecond respectively [14].

$$V_\alpha = \left\{1 - \frac{1}{\left(\frac{m_\alpha + E_\alpha}{m_\alpha}\right)^2}\right\}^{1/2} \times V_{gamma} \qquad \text{Eqn.3.5}$$

$$V_n = \left\{1 - \frac{1}{\left(\frac{m_n + E_n}{m_n}\right)^2}\right\}^{1/2} \times V_{gamma}$$

Where velocity of gamma V_{gamma}=30 cm/nanosecond

Mass of alpha particle m_α =3737.37911 MeV/c^2

Mass of neutron particle m_n =939.56536 MeV/c^2

Energy of alpha particle E_α =3.5 MeV

Energy of neutron particle E_n =14.1 MeV

Using the principles of Euclidean geometry and knowing the geometrical correlations between an alpha particle and the tagged neutron, the time stamping of gamma-rays and their energies registered by Geant4, and from the known velocities of the 14.1 MeV neutron (5.1 cm/ns) and gamma-rays (30 cm/ns), the ROOT software was used to re-construct 2D and 3D images of the hypothetical UXO object. The Equation set Eqn.3.6~3.8 is the core algorithm in our code run by ROOT. From the equation set, the reaction point within the UXO along a neutron beam (x_n, y_n, z_n) can therefore be obtained. Then, we can plot the UXO in 2D and 3D (Fig.3.15).

$$d_n = \sqrt{x_n^2 + y_n^2 + z_n^2} \approx t_g \times V_n \qquad \text{Eqn.3.6}$$

$$d_\alpha = \sqrt{x_a^2 + y_a^2 + z_a^2} \qquad \text{Eqn.3.7}$$

$$\frac{x_n}{x_a} = \frac{y_n}{y_a} = \frac{z_n}{z_a} = \frac{d_n}{d_\alpha} \qquad \text{Eqn.3.8}$$

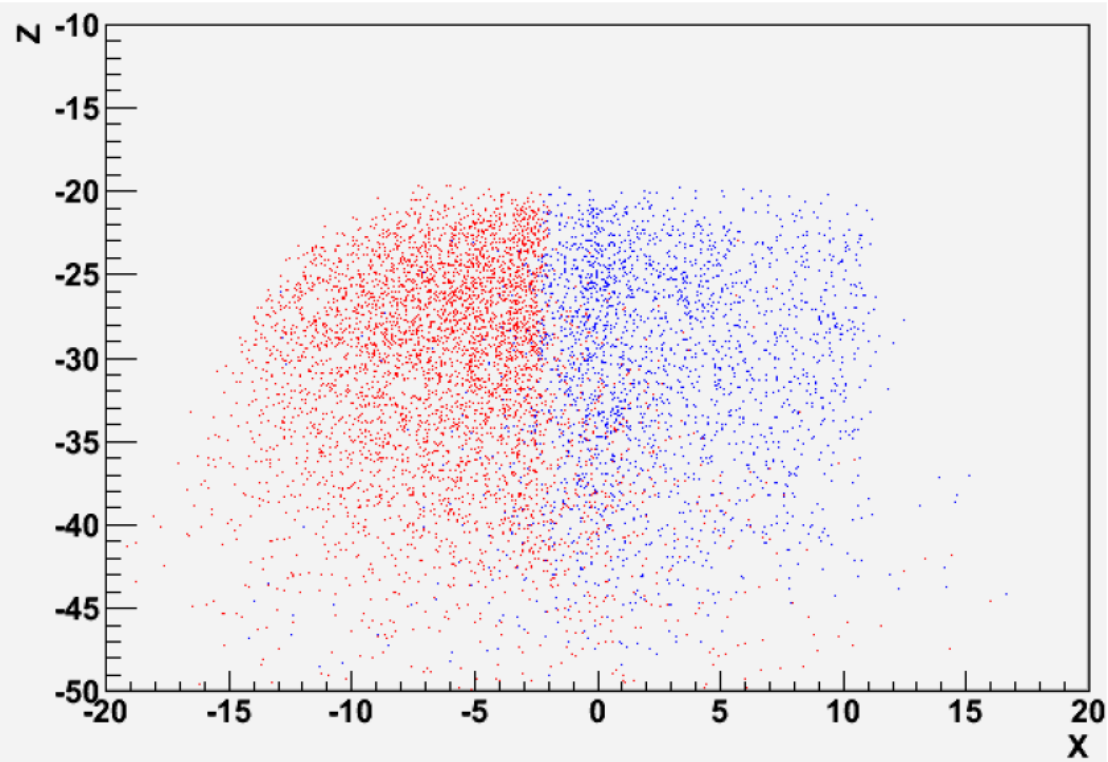

Figure 3.15: 2D image reconstruction of the hypothetical UXO correctly showing it positioned 20 cm away from the neutron production site in the z direction. The carbon and oxygen densities have also been isolated in their respective halves using the 4.43 and 6.13 MeV gamma lines respectively.

The algorithm correctly located the object placed 20 cm away from the neutron production site along with its length of 25 cm and reconstructed it with the elemental densities of C and O in their respective halves as designed in the experiment.

Chapter 4

4 Monte Carlo Simulations of Prompt Gamma-ray Spectra Induced by Tagged Neutrons

4.1 Spectrum of Energy Deposited by Gamma-rays Undergoing Electromagnetic Processes

All the simulations in this section are conducted on Geant4 platform installed on Linux. The main physical processes implemented in this chapter are standard electromagnetic and hadronic processes. The hadronic processes here are the same as in the previous chapters. As to electromagnetic processes, they are introduced only for three kinds of particles: gamma, electron, and positron.

- Gamma: photoelectric effect, compton scattering, gamma conversion
- Electron: multiple scattering, ionisation, bremsstrahlung
- Positron: multiple scattering, ionisation, bremsstrahlung, plusannihilation

To first have a brief view of the electromagnetic processes in Geant4, a point gamma source was placed at 5 cm distance in front of a NaI detector [15] with diameter and length both at 12.7 cm (Fig. 4.1). The simulation world was filled with vacuum, which, in our Geant4 codes, was defined as atomic number 1, mass of mole 1.008 g/mole, density 1.e-25 g/cm^3, kStateGas, temperature 2.73 kelvin, pressure 3.e-18 pascal. 1,000,000 gamma rays were generated.

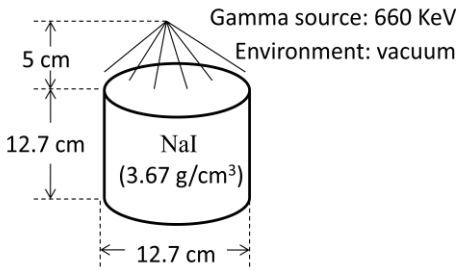

Figure 4.1: Simulation layout showing gamma source of energy 660 KeV is placed 5 cm away from the NaI detector of dimension 12.7 x 12.7 cm

In Geant4, an event is generated using the method generatePrimaries(), in which you may define the particle to be generated, particle numbers, particle energy, particles generation position, particle momentum direction, and so on. In the following of the event, the information of detector response is recorded in the minimum unit: step. It includes two end points: PreStepPoint and PostStepPoint. Another concept is hit. A hit can store any combinations of the step information [16]:

- the position and time of the step
- the momentum and energy of the track
- the energy deposition of the step
- geometrical information

In our applications, there was one gamma ray generated in the beginning of each event. A hit was defined as a set of 2 info in a step: the energy deposited in the step, and global PreStepPoint time (time from the beginning of current event to the PreStepPoint). The Global PreStepPoint time of the first step in an event was used as t_g. The alpha-gamma coincidence time spectrum was plotted by using t_g of all the events. Gamma rays might undergo a series of interactions with the matters, resulting in ejected electrons and positrons, and all of which might deposit energy in

the detector through separate steps. Thus, the total energy deposit per incident gamma ray, E_g, was the sum of the deposited energy from all the steps. The summation was completed by retrieving the hits collection in the end of each event. E_g was then used to plot the prompt gamma-ray energy spectrum (Fig. 4.2).

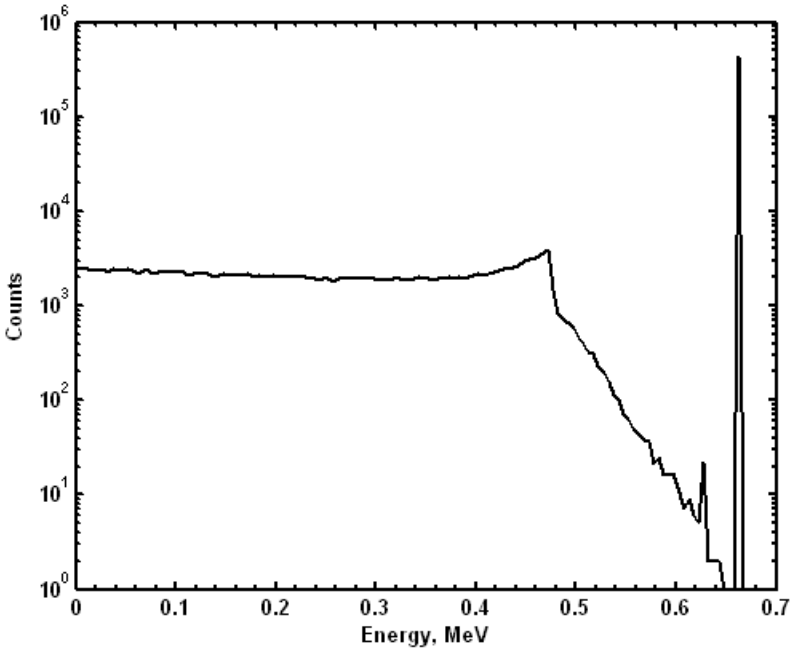

Figure 4.2: Energy deposited by gamma rays of energy 660 KeV in the NaI detector

4.2 Simulations of 14.1 MeV Neutron-induced Prompt Gamma-ray Spectra from Elements and Materials

With this simple test quickly done, we proceeded to simulate the spectra of the most important elements for explosive identification, carbon, nitrogen and oxygen. As before, all components of the system were placed within a 3D world volume filled with vacuum. The neutron and alpha production site was placed at the origin of the world volume using an x, y and

z Cartesian coordinate system where the z axis was the neutron and alpha directions. Using particle guns designed in the Geant4 primary generator, a neutron of energy 14.1 MeV and its associated alpha particle with energy 3.5 MeV were generated at the same time and in opposite directions. The azimuthal angle φ of both particles was uniformly distributed and generated randomly within 360^0. The cone angle θ_n was constrained to be no larger than $\pm 7.83^0$ (The angle was designed to make the neutron-beam cone cover the whole sample body). For all experiments, 1,000,000 alpha-neutron pairs were used in each run. The computation time was ~5 minutes for each run. An alpha-particle detector made up of plastic and having a diameter of 15 cm and thickness 1 cm was placed at the position (0,0,-30) cm and four NaI gamma-ray detectors each of diameter and thickness both at 12.7 cm (5 in) were positioned at (30,0,75) cm, (-30,0,75) cm, (0,30,75) cm, and (0,-30,75) cm relative to the origin of the world volume. The detectors were also defined to be sensitive so that once a particle entered the detectors, they recorded all the necessary hit information such as position and time. The object-of-interest was 15cm x 15 cm x 10 cm thick and placed 80 cm from the neutron production site (Fig. 4.3).

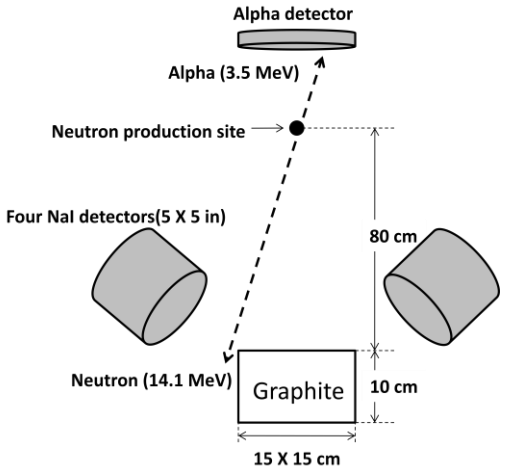

(a)

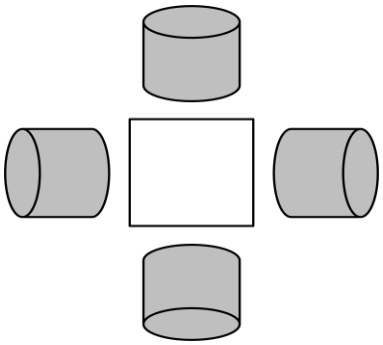

(b)

Figure 4.3: (a) side view and (b) top view of the environment for element spectra simulations

Figure 4.4 presents a typical alpha-gamma coincidence time spectrum acquired with the graphite sample, which was represented by C with density 1.2 g/cm^3. The origin of the time axis corresponded to the neutron source (tritium target), and the main prompt coincidence peak corresponded to the gamma rays produced in the sample. The second peak was due to neutrons scattered inside the sample, hitting the detectors, and then producing a signal inside the NaI crystal [17, 18]. We can find the two time-of-flight peaks were separated by ~6 ns as predicted from theory, because the distance between the centroids of the detectors and the graphite object was ~30 cm, and the speed of a 14.1 MeV neutron is 5.1 cm/ns. The 16-20 ns time window was chosen to minimize the scattered-neutron contribution in the gamma-ray spectrum of the sample. The result is presented in Figure 4.5

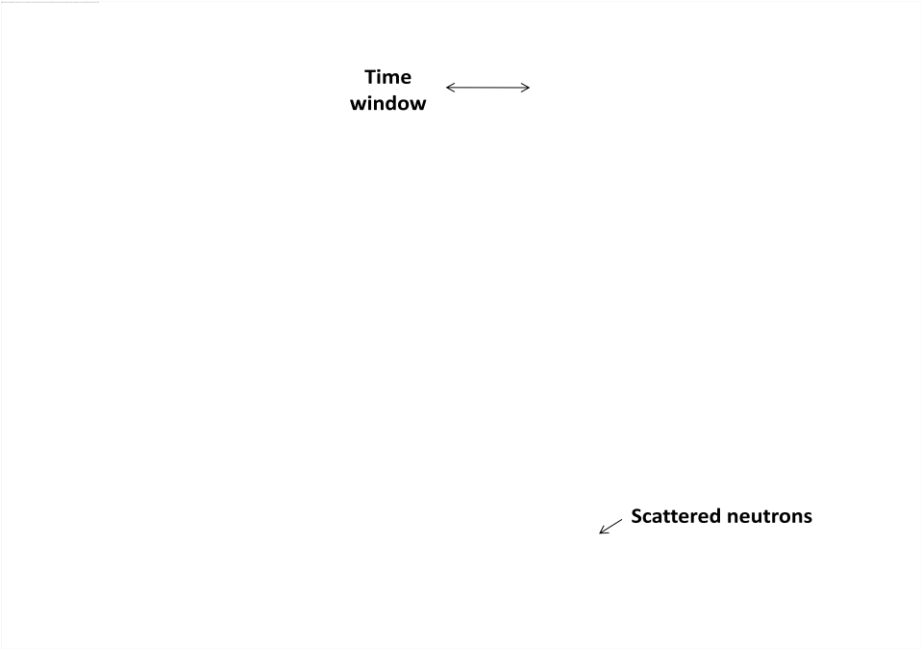

Figure 4.4: The alpha-gamma coincidence time spectrum recorded by the NaI detectors

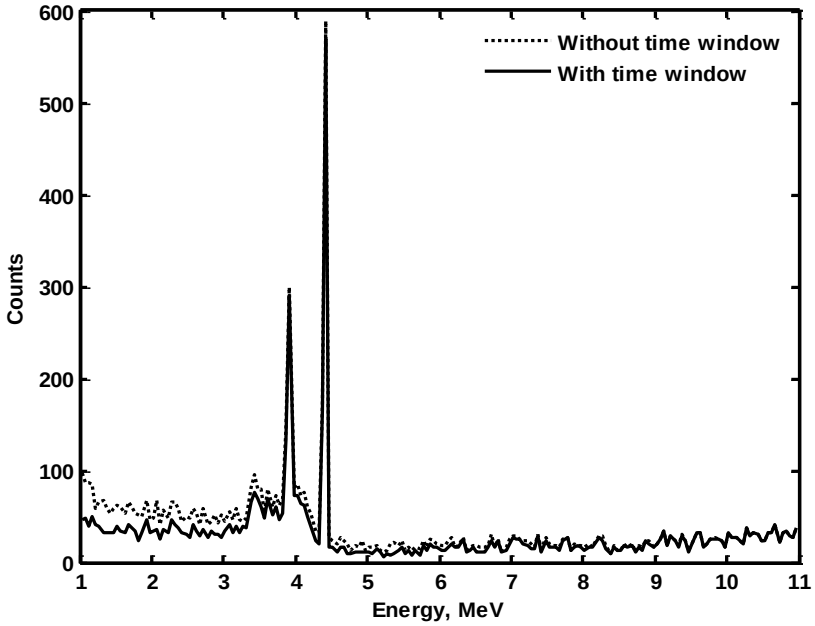

Figure 4.5: Simulated gamma-ray spectra of graphite

The oxygen spectrum was measured with the water sample of density 1.0 g/cm^3 (Fig. 4.6). It can be noted that there was a sharp peak at around 2.2 MeV when time window was not applied.

The time spectrum of the peak (Fig. 4.7) showed that many of its constituents occurred much later than the time window set for the sample body. The spectrum of solid oxygen (1.43 g/cm^3) is also presented for comparison (Fig.4.8).

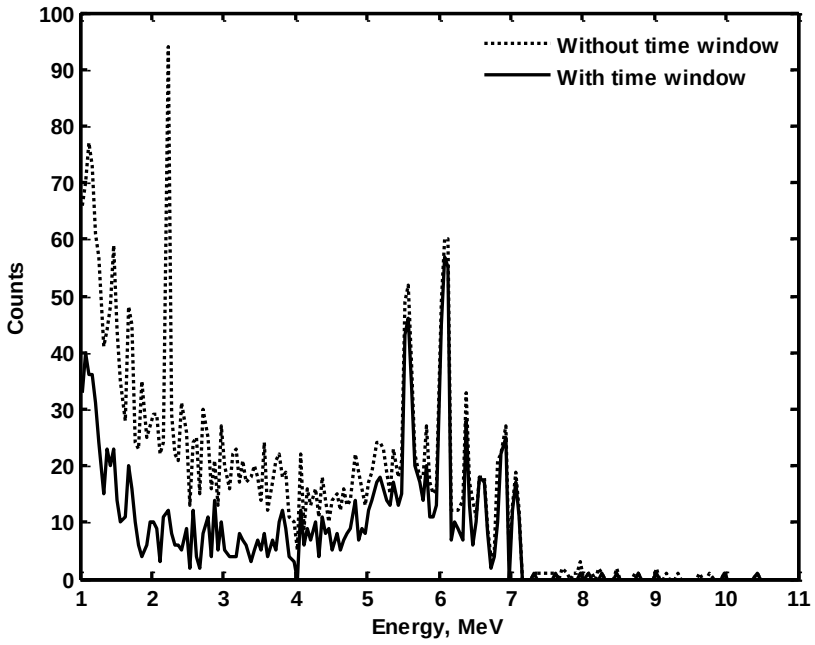

Figure 4.6: Simulated gamma-ray spectra of water

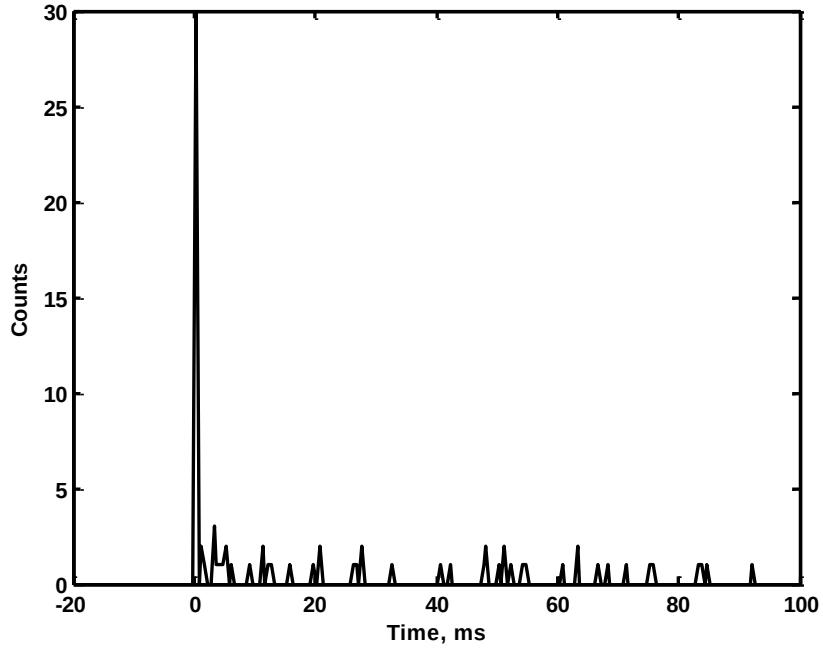

Figure 4.7: Time spectrum of the 2.2 MeV peak in the gamma-ray spectrum of water

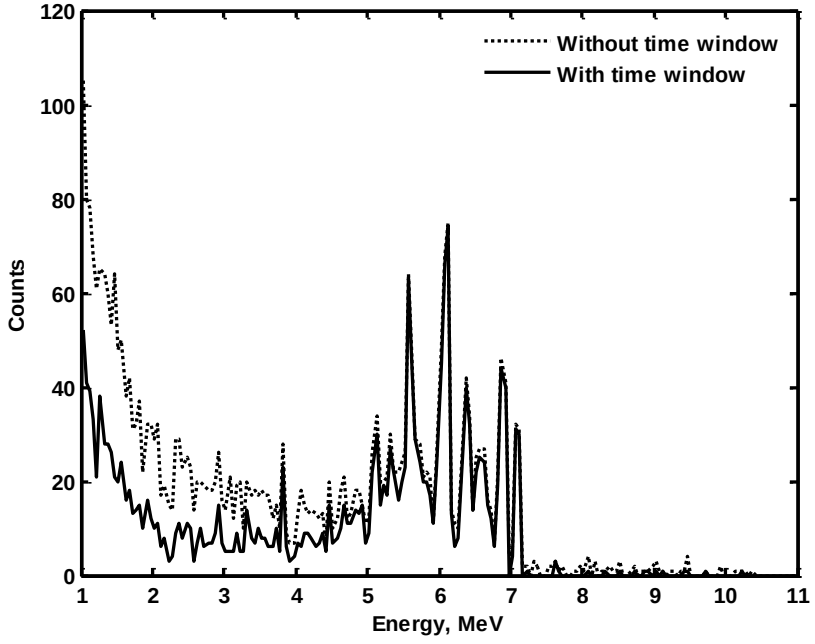

Figure 4.8: Simulated gamma-ray spectra of solid oxygen

In the simulation of nitrogen spectrum, melamine ($C_3H_6N_6$) of density 0.74 g/cm^3 was measured at first according to W. El Kanawati et al. [17]. Since it contains carbon, a fraction of 20%

of the carbon spectrum was subtracted from the melamine spectrum to derive the nitrogen spectrum (Fig. 4.9). Both the melamine and carbon spectra used here were the ones after subtraction of the scattered neutron signals with time window. The spectrum of solid nitrogen (1.026 g/cm^3) is also presented for comparison (Fig.4.10).

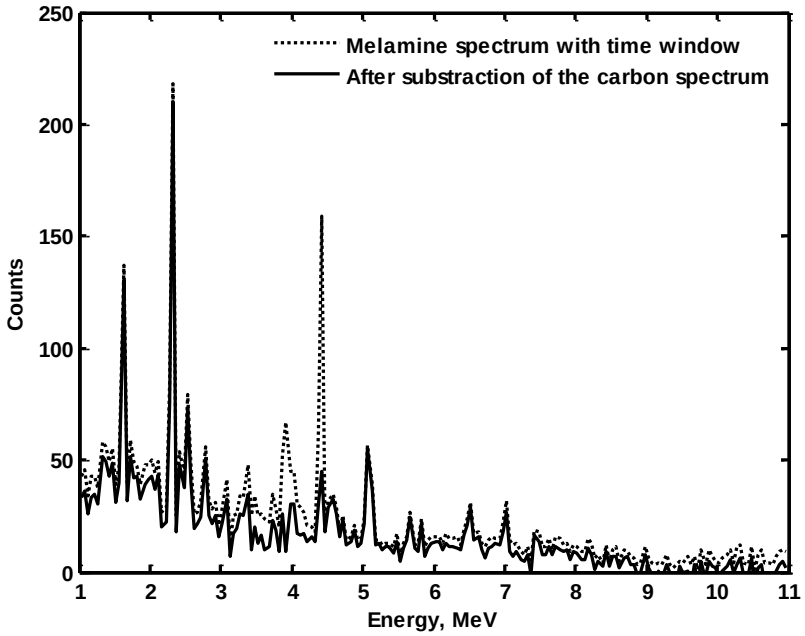

Figure 4.9: Simulated gamma-ray spectra of nitrogen from a melamine sample

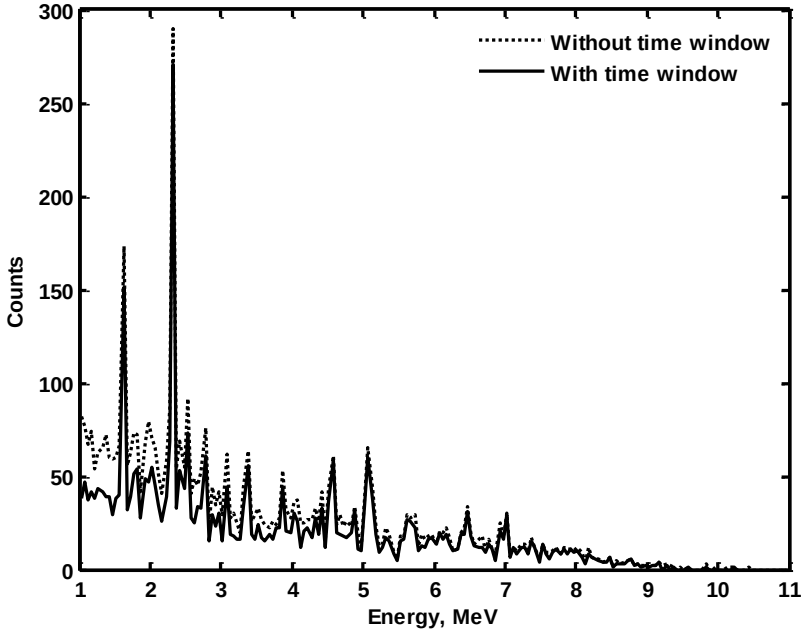

Figure 4.10: Simulated gamma-ray spectra of solid nitrogen

In addition to the elemental spectra, those of three kinds of materials, hexogen ($C_3H_6O_6N_6$), nylon ($C_{11}H_{26}O_4N_2$) and PAN (C_3H_3N), with densities of 1.8, 1.15 and 1.18 g/cm^3 separately, were simulated in our study (Fig. 4.11, 4.12, and 4.13). They have similar element constituents; Difference is that hexogen is a kind of common High Explosives, while nylon and PAN are innocuous materials. The next chapter will address the ability of neural networks to differentiate explosives from innocuous materials with similar element constituents.

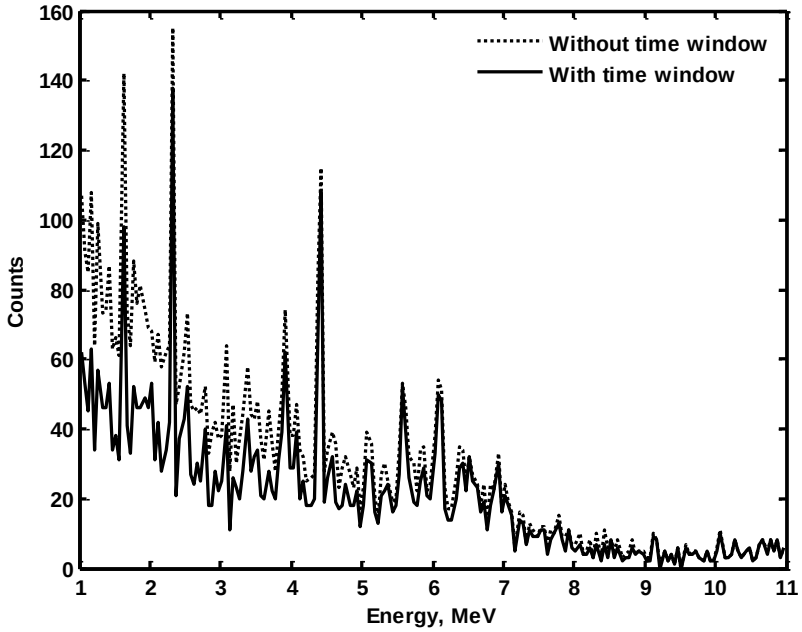

Figure 4.11: Simulated gamma-ray spectra of hexogen

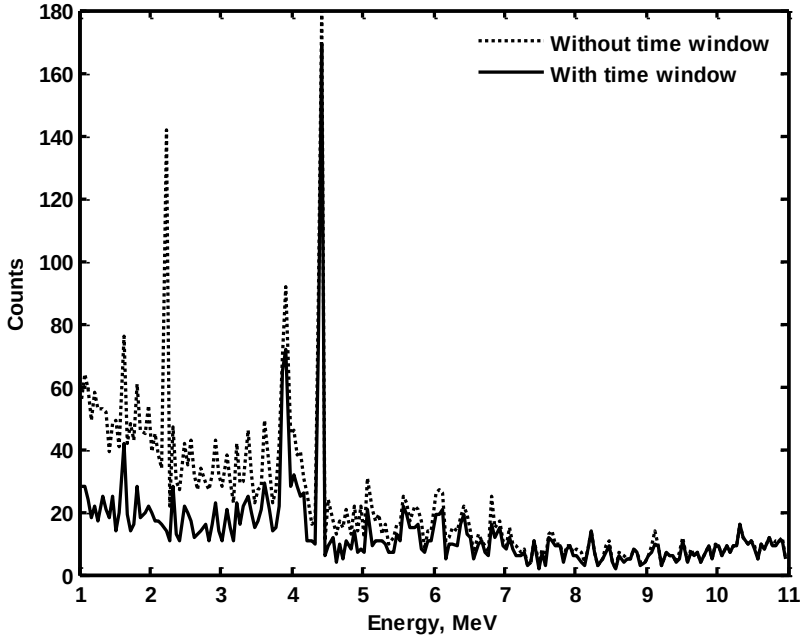

Figure 4.12: Simulated gamma-ray spectra of nylon

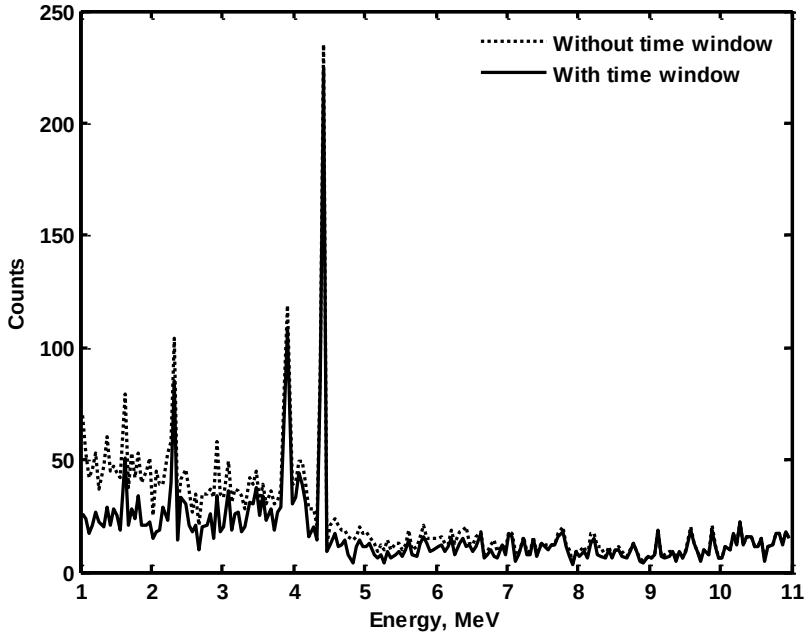

Figure 4.13: Simulated gamma-ray spectra of PAN

Chapter 5

5 Identification of Materials Using Neural Networks

5.1 Introduction of Neural Networks

Neural networks are mathematical models inspired by the biological nervous systems, and they possess the capacity to extract knowledge from a group of data previously established [19]. A network is composed of simple elements, called neurons, which are operating in parallel. As in nature, the network function is determined largely by the connections between neurons. A typical neuron model is shown in Figure 5.1.

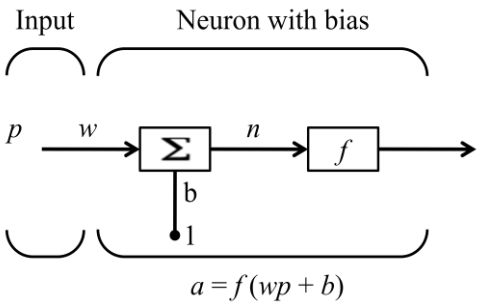

Figure 5.1: Model of a neuron

The scalar input p is transmitted through a connection that multiplies its strength by the scalar weight w. Some neurons have a scalar bias, b, which is much like a weight and has a constant input of 1. The bias can be viewed as simply being added to the product wp by the summing junction or as shifting the function f to the left by an amount b. This sum is the argument of the transfer function f. Transfer function is typically a step function or a sigmoid function, which produces the output a. Two or more of the neurons can be combined in a layer

(Fig. 5.2). Here the input p is a vector of R input elements. These inputs post-multiply the S-row, R-column matrix W. S represents of number of neurons in a layer. As before, a constant 1 enters as an input and is multiplied by the bias number of each neuron separately. Note that the network output is a vector, with each element corresponding to the output of each neuron. A network can have several layers. The layer that produces the network output is called the output layer. All other layers are called hidden layers.

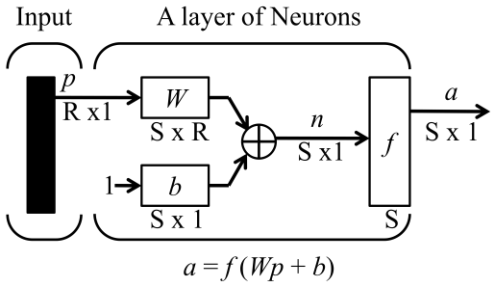

Figure 5.2: Model of a layer of neurons

Note that w and b are both adjustable scalar parameters of the neuron. The central idea of the neural network is that we can train it to perform a desired behavior by adjusting such parameters during presentation of individual input vectors. By comparing the network output with the target, the adjusting is conducted until the output matches the target. The process is shown in Figure 5.3. Typically many such input/target pairs are needed to train a network.

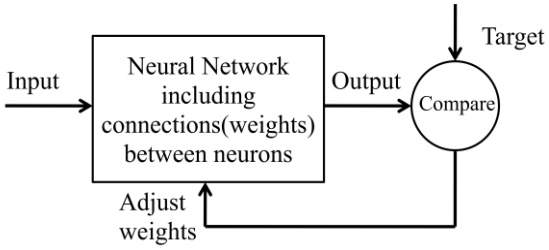

Figure 5.3: Training principle of a neural network

Neural networks have a history of some six decades but have found solid application only in the past twenty years. Currently, neural networks have been trained to perform complex functions in various fields, including pattern recognition, identification, classification, speech, vision, and control systems. As the gamma-ray energy spectra can be considered as patterns, it is interesting to use the neural networks to perform material identification. V. Doostmohammadi et al. [20] simulated the neutron capture prompt gamma-ray spectra of various samples by MCNP, and developed neural networks to sense what kinds of elements exist in each sample. W. Nunes et al. [21] applied a neural network to determine the presence of C4 when it was occluded by several materials, using the simulated gamma-ray spectra of the substances as patterns. F. Ferreira et al. [22] obtained the real time neutron radiographic (RTNR) images of samples such as drugs, plastic explosives and ordinary materials through an electronic imaging system, and used them to train the neural works in order to classify and identify the suspicious ones. In our study, several networks were designed by Neural Network Toolbox 7 of Matlab [23] to reveal the potential in the identification of gamma-ray spectra.

5.2 Establishment of Neural Networks and Performance Evaluation

- Model 1: The first network was developed to identify each of the presented materials: hexogen, nylon and PAN.

The spectrum of a material had 200 bins of energy from 1.0 to 11.0 MeV, with bin width of 0.1 MeV each. The count numbers of all the bins were read into Matlab to form a 200-element

column vector, called input vector, which represented one of the 3 materials. The target vector was a 3-element column vector, with a 1 in the position of the material it represented, and 0's everywhere else. Each output vector represented a material. For example, “hexogen” was represented by a vector with 1 in the first element, “nylon” by a 1 in the second, and “PAN” by a 1 in the third. The network received the 200 count numbers as an input pattern, and then identified the pattern by responding with a 3-element output vector. To operate correctly, the network should respond with a 1 in the position of the material being presented to the network, and 0’s in all others. When it came to the structural implementation, there were two layers in our network (Fig. 5.4). It had 200 neurons in the input (hidden) layer, each corresponding to the 200 bins of an input spectrum, and 3 neurons in the output layer to represent the 3 materials. The network was of feed-forward backpropagation type. The log-sigmoid transfer function was picked for each layer because its output range, 0~1, is perfect for learning to output boolean values. Adaption was done by updating weights with the specified learning function “learngdm”. Training was done with the specified training function “traingdx”, adaptive learning rate of 0.01 and momentum of 0.95. Performance was measured according to sum-squared error performance function.

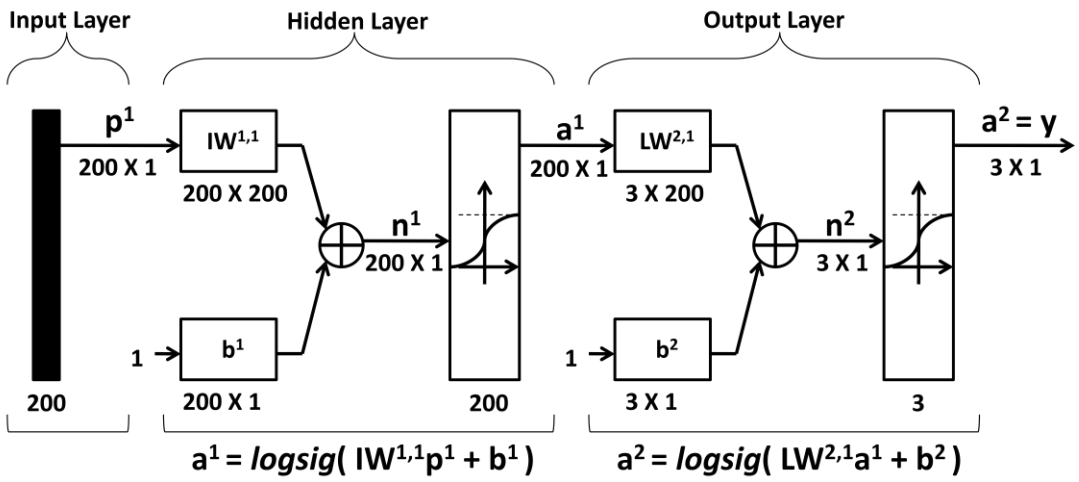

Figure 5.4: Two-layer network of model 1

The network was initially trained with one set of ideal input (one set consisted of 3 vectors, each representing one kind of materials among hexogen, nylon and PAN) for a maximum of 5000 epochs or until the network sum-squared error fell beneath 0.1. But this was not enough in that the network should yet be able to handle some noise, but not be too sensitive. With this in mind, we continued training with 4 sets of input at the same time, two ideal ones and two noisy ones. Each noisy set was an ideal one to which was added a matrix, with the same dimension as an ideal set, but values from normal distribution of mean 0, and standard deviation of 15 and 25 respectively. This forced the neuron to learn how to properly identify noisy sets, while still respond well to ideal ones. The four-sets-a-time training underwent 10 times. After that, it made sense to train with an ideal set once more to ensure that ideal inputs could always be classified correctly. The whole process is listed in Table 5.1.

Table 5.1: Training process of the neural network of model 1

Training Process			
Step	1	2	3
Epoch number	5000	300	500

Sum-squared error goal	0.1	0.1	0.1
input-sets in a training cycle	1 ideal-set	2 ideal-sets and 2 noisy-sets	1 ideal-set
Number of training cycle	1	10	1
NOTE: 1 input-set consists of 3 vectors, each representing one kind of materials among hexogen, nylon and PAN			

The reliability of the pattern recognition system was measured by testing the network with hundreds of sets of input with varying quantities of noise. In detail, noise with a mean of 0 and a standard deviation from 0 to 50 was added to respective input-sets. At each deviation level, 1000 different versions of noise matrixes were randomly made and the network's output was calculated. Noisy inputs may result in the network not creating perfect 1's and 0's. Thus, the output was passed through the competitive transfer function “compet”. This made sure that the output corresponding to the material most like the noisy input vector took on a value of 1, and all others had a value of 0. The percentage of recognizing error in different cases is plotted in Figure 5.5, 5.6 and 5.7. The performance of the network only trained without noise is also showed for comparison.

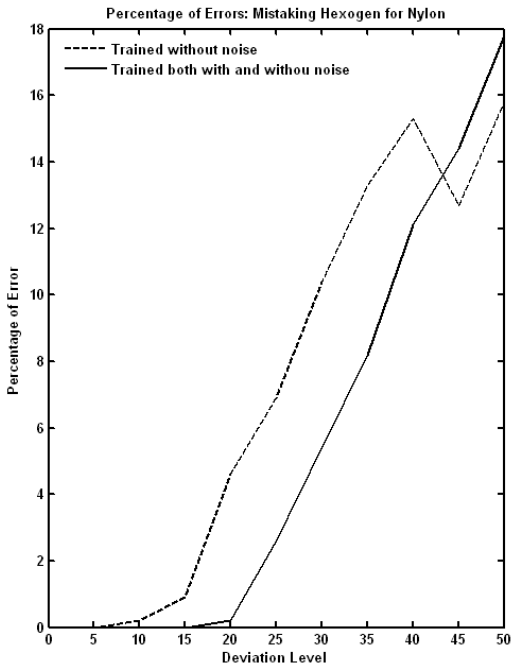

(a)

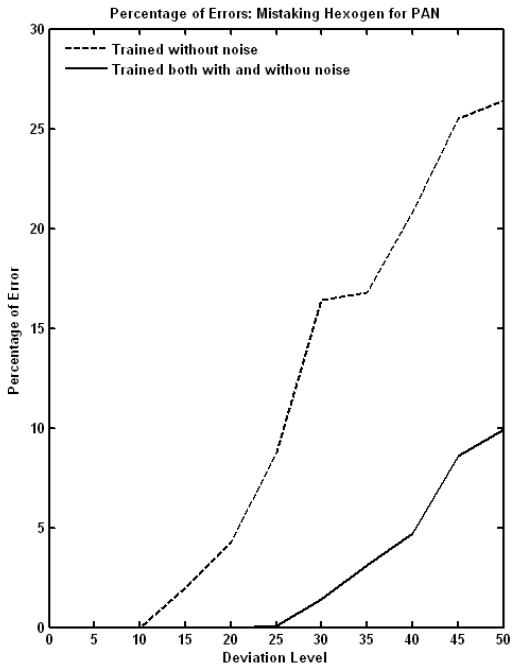

(b)

Figure 5.5: Percentage of error of (a) mistaking hexogen for nylon, and (b) mistaking hexogen for PAN

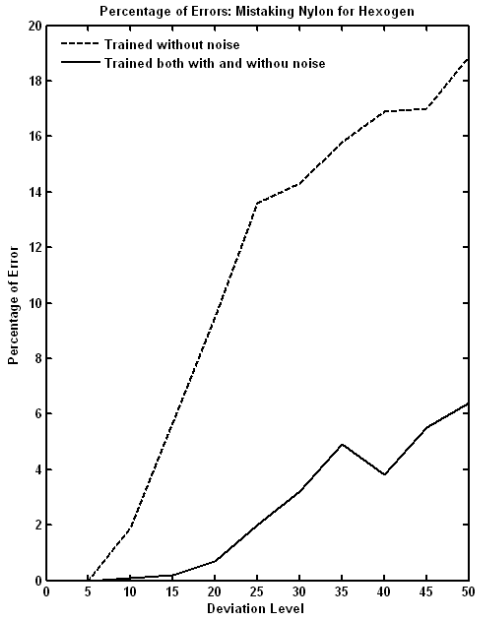

(a)

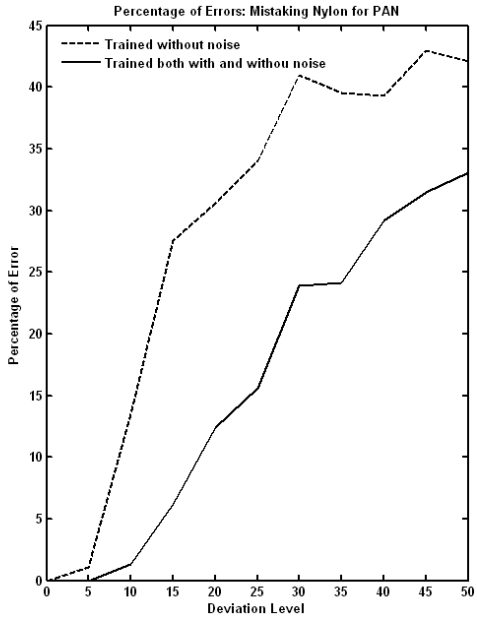

(b)

Figure 5.6: Percentage of error of (a) mistaking nylon for hexogen, and (b) mistaking nylon for PAN

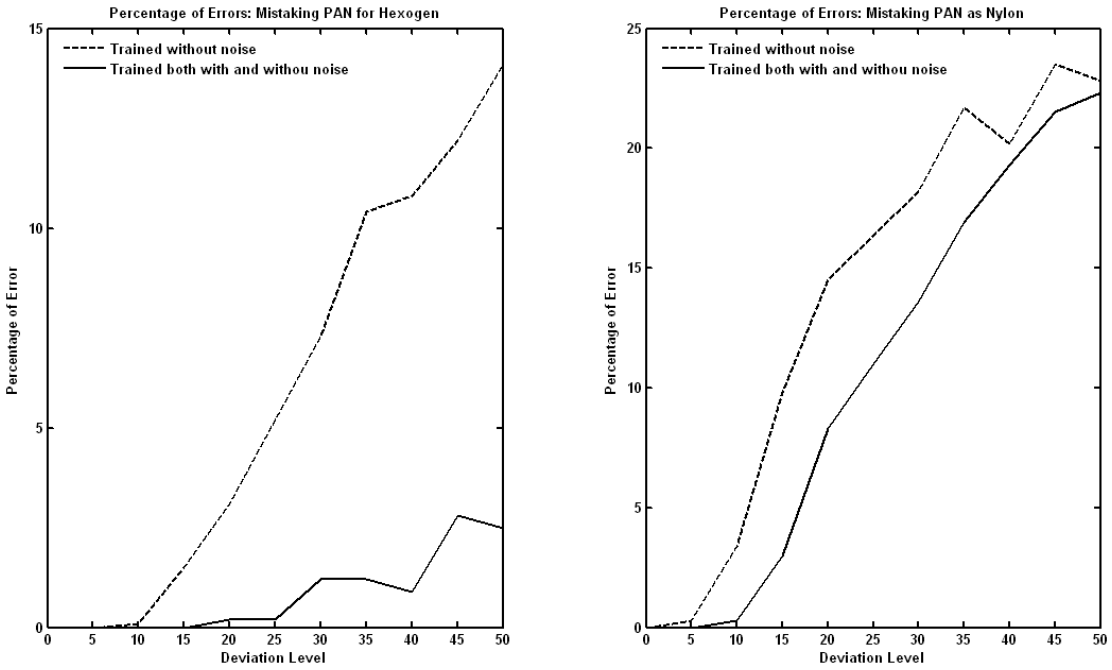

(a) (b)

Figure 5.7: Percentage of error of (a) mistaking PAN for hexogen, and (b) mistaking PAN for nylon

We knew that the two photon energy characteristics that possessed weights of great importance to the recognition of explosives, were associated with the presence of C and N. So, we chose hexogen ($C_3H_6O_6N_6$), nylon ($C_{11}H_{26}O_4N_2$) and PAN (C_3H_3N) as sample materials. Though all containing C and N, Hexogen is explosive, while nylon and PAN are innocuous materials. The key resides in the fact that High Explosive presents a high concentration of the element of N, which differentiates it from other materials with hydrogen content. Materials such as nylon or PAN possess atoms of N, but in much smaller concentrations, in relation to the number of atoms of C. It was interesting to see whether the network can tell the explosive from the innocuous based on the relative amount. As predicted, nylon and PAN were less likely to be mistaken for hexogen, than for each other (Fig. 5.6 and 5.7). That was because the N signal of

the explosive, hexogen, was much stronger than that of the innocuous materials, nylon and PAN. It can also be noted that hexogen was more likely to be mistaken for nylon than PAN (Fig. 5.5). That was because the spectrum of nylon, like that of hexogen, had more relative counts of C than PAN. This factor also accounted for much in explosive pattern recognition. In addition, the presence of oxygen in nylon may play a role as well.

In general, the network had much better performance than if only trained without noise. The percentage of error was rather small even when the deviation level of noise increased to 15.

- Model 2: The second network was designed to determine the presence of hexogen, in spite of the presence of occluding materials, nylon and PAN.

The hexogen sample was 15 cm x 15 cm x 10 cm thick and placed 80 cm away from the neutron production site, same as before. However, innocuous materials, nylon and PAN, of different thicknesses were added layer-wise towards the neutron production site (Fig.5.8). For the experiment of each thickness setting, 1,000,000 neutrons were generated.

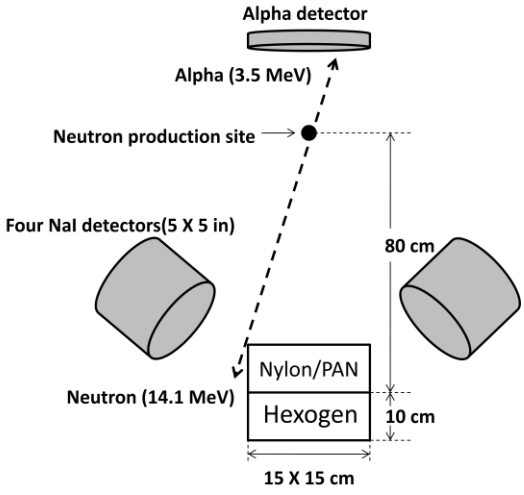

Figure 5.8: Simulation environment of input spectra for the neural network of model 2

The spectra of hexogen hidden by nylon and PAN with different thicknesses (including thickness of 0), were presented as the input patterns for neural network of model 2. Their corresponding target vector was a 2-element column vector, $(1\ 0)^T$, representing the presence of hexogen. The spectra of pure nylon and PAN of model 1 were also used as input patterns, and the corresponding target vector was $(0\ 1)^T$, representing the absence of hexogen. The network structure was different from that of model 1 only in the neuron numbers of output layer (Fig.5.9).

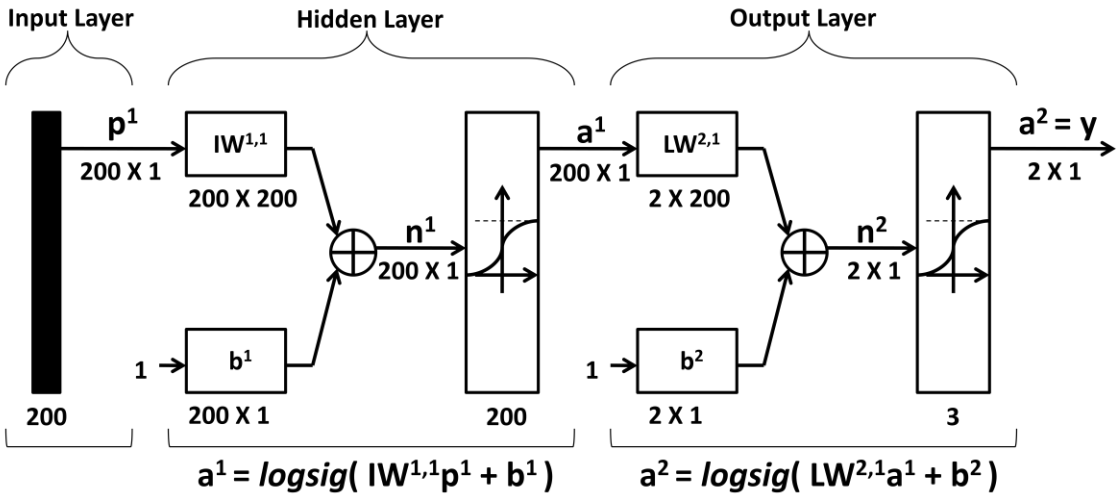

Figure 5.9: Two-layer network of model 2

The training process is listed in Table 5.2.

Table 5.2: Training process of the neural network of model 2

Training Process			
Step	1	2	3
Epoch number	5000	300	500
Sum-squared error goal	0.1	0.1	0.1
input-sets in a training cycle	1 ideal-set	1 ideal-set, hexogen hidden by 4 cm nylon and hexogen hidden by 4 cm PAN	1 ideal-set
Number of training cycle	1	10	1

NOTE: 1 ideal-set consists of 3 vectors, representing pure hexogen, nylon and PAN, respectively

The performance was measured by testing the network with spectra of pure nylon and PAN, and spectra of hexogen hidden by nylon and PAN with thicknesses from 0 to 10 cm. The output was passed through the competitive transfer function "compet". The network recognized the presence and absence of hexogen with 0 percentage of error. In contrast, the network trained only with a set of pure hexogen, nylon and PAN cannot recognize hexogen when the thickness of occluding materials increased.

Chapter 6

6 Conclusion

In this thesis, the Geant4 Monte Carlo toolkit has been successfully implemented to simulate a preliminary UXO sensing model. Based on the associated-particle neutron time-of-flight technique, the simulation results suggest that with the vastly improved signal-to-noise ratios of measuring elemental densities, UXOs can be identified even when buried in the sub-surface to 20 cm depths. This is not possible with any existing neutron interrogation technique. This technique also presents advantage of image reconstruction. With the help of alpha-gamma coincidence time, the scattered neutron contribution to the gamma-ray spectra can be reduced. The neural networks are proved to be effective in the pattern recognition of the simulated spectra of explosives as well as innocuous materials.

Future work will involve benchmarking the simulation results with laboratory experiments that will include simulations with realistic detector sizes and instrumental time resolutions, neutron generator dimensions and detailed gamma-ray interactions in a detector to synthesize gamma-ray spectra. It is envisioned that validation of the simulation environment will allow rapid design and development of a functional UXO sensing instrument.

Bibliography

[1] R. Moyes, 2005. Landmine Action. “Explosive remnants of war and mines other than anti-personnel mines”. Report of Landmine Action, Landmine Action, London, UK.

[2] Office of the Under Secretary of Defense, 2003. “Unexploded Ordnance”. Report of the Defense Science Board Task Force, Washington, D.C., United States.

[3] A. Buffler, F.D. Brooks, M.S. Allie, K. Bharuth-Ram and M.R. Nchodu, 2001. “Material classification by fast neutron scattering”. Nucl Instrum Methods Phys Res Sect B 173(4): 483-502.

[4] P.C. Womble, F.J. Schultz and G. Vourvopoulos, 1995. “Non-destructive characterization using pulsed fast-thermal neutrons”.Nucl Instrum Methods Phys Res Sect B 99(1-4):757-760.

[5] S. Mitra, J.E. Wolff, R. Garrett and C.W. Peters, 1995. “Application of the associated particle technique for the whole-body measurement of protein, fat and water by 14 MeV neutron activation analysis- a feasibility study”. Phys Med Biol 40(6): 1045-1055.

[6] D.L. Chichester, M. Lemchak and J.D. Simpson, 2005. “The API 120: A portable neutron generator for the associated particle technique”. Nucl Instrum Methods Phys Res Sect B 241(1-4): 753-758.

[7] D. Sudac, S. Pesente, G. Nebbia, G. Viesti and V. Valkovic, 2007. “Identification of materials hidden inside a container by using the 14 MeV tagged neutron beam”. Nucl Instrum Methods Phys Res Sect B 261(1-2):321-325.

[8] S. Agostinelli et al., 2003. “GEANT4-A simulation toolkit”. Nucl Instrum Methods. Phys Res Sect A 506(3):250-303.

[9] J. Allison et al., 2006. “Geant4 Developments and Applications”. IEEE Transactions on Nuclear science 53(1): 270-278

[10] Geant4 Collaboration. Geant4 Installing Guides. http://geant4.slac.stanford.edu/installation/

[11] Jeffrey Freidberg, 2007. “Plasma Physics and Fusion Energy”. Cambridge University Press, Cambridge, United Kingdom.

[12] J. Benveniste and J. Zenger, 1954. “Information on the Neutrons Produced in the H3(d,n)He4 Reaction”. Report of Atomic Energy Commission, United States.

[13] J.F. Sutcliffe, A.H. Smith, A.J. Waker, M.C.J. Barker and M.A. Smith, 1991. “Inelastic scattering of pulsed 14.4 MeV neutrons as a function of depth in tissue and the halflife for radiative capture”. Phys.Med.Biol. 36(5):643-648.

[14] G.W. Carriveau, 2006. “Associated Particle Imaging: An Enabling Technology of Detection of Improvised Explosive”. Detection and Disposal of Improvised Explosives. NATO Security through Science Series, 123-125

[15] Katja Roemer et al., 2006. “Simulation of Template Spectra for Scintillator Based Radionuclide Identification Devices Using GEANT4”. 2006 IEEE Nuclear Science Symposium Conference Record

[16] Geant4 Collaboration. Geant4 User's Guide for Application Developers. Website. http://geant4.web.cern.ch/geant4/UserDocumentation/UsersGuides/ForApplicationDeveloper/html/index.html

[17] W. El Kanawati et al., 2011. “Acquisition of prompt gamma-ray spectra induced by 14 MeV neutrons and comparison with Monte Carlo simulations”. Appl. Radiat. Isotopes, doi:10.1016/j.apradiso.2011.01.010

[18] B. Perot et al., 2008. “Measurement of 14MeV neutron-induced prompt gamma-ray spectra from 15 elements found in cargo containers”. Applied Radiation and Isotopes 66:421-434

[19] S. Haykin, 1999. “Neural Networks: a Comprehensive Foundation”. Prentice Hall, Englewood Cliffs, NJ.

[20] V. Doostmohammadi et al., 2010. “Combined application of Monte Carlo method and neural networks to simulate qualitative prompt gamma neutron activation analysis”. J Radioanal Nucl Chem 283:403-407

[21] W. Nunes et al., 2002. “Explosives detection using prompt-gamma neutron activation and neural networks”. Applied Radiation and Isotopes 56: 937-943

[22] F. Ferreira et al., 2010. “Detection of drugs and explosives using neutron computerized tomography and artificial intelligence techniques”. Applied Radiation and Isotopes 68: 1012-1017

[23] M.H. Beale, M.T. Hagan and H.B. Demuth, 2010. “Neural Network Toolbox 7 User’s Guide”. MathWorks.